PRE-TRANSFORMATION PHENOMENA

IN THE

INTERMETALLIC COMPOUND TiNi

PRE-TRANSFORMATION PHENOMENA

IN THE

INTERMETALLIC COMPOUND TiNi

by

KULDEEP CHANDRA, B. TECH.(HONS.)

A Thesis

Submitted to the Faculty of Graduate Studies

in Partial Fulfilment of the Requirements

for the Degree

Master of Engineering

McMaster University

January 1967

MASTER OF ENGINEERING (1967)
(Metallurgical Engineering)

McMASTER UNIVERSITY
Hamilton, Ontario

TITLE: Pre-transformation Phenomena in the Intermetallic Compound TiNi

AUTHOR: Kuldeep Chandra, B. Tech. (Hons.)

SUPERVISOR: Dr. G. R. Purdy

NUMBER OF PAGES: ix, 66

SCOPE AND CONTENTS:

Prior work in this system has indicated that, under favourable conditions, the formation of a martensitic transformation product on cooling may be preceded by a second-order cubic-rhombohedral transformation. In the present investigation, thin film electron microscopy and diffraction have been employed to study the pre-transformation phenomena in the temperature range 20 - 300°C. The results are interpreted in terms of localized thermal diffuse scattering, resulting from incipient mechanical instability. A model for the cubic-rhombohedral transformation, in terms of lattice dynamics, is suggested. Dark field micrographs of the rhombohedral phase suggest a moderate degree of co-operation between adjacent domains. Additional data is provided in the form of volumetric and x-ray intensity measurements.

ACKNOWLEDGEMENTS

The author wishes to express his sincere gratitude to Dr. G. R. Purdy for the invaluable advice provided by him in the solution of this problem, and his able supervision of the entire work.

Gratitude must also be expressed to Mr. Harry Walker for the troubles taken in the frequent installations of heating stage in the electron microscope for this work.

The financial support of the National Research Council of Canada is gratefully acknowledged.

TABLE OF CONTENTS

	Subject	Page
CHAPTER I	Introduction	1
CHAPTER II	Literature Review	2
CHAPTER III	Theory of Second Order Transformations and Thermal Diffuse Scattering	5
3.1	Introduction - Transformation Types and Their Speeds	5
3.2	Landau's Theory of Second Order Transitions	6
3.3	Tisza's Theory of Second Order Transitions	8
3.4	Quasi-Thermodynamic Formalism of Tisza and Klein	10
3.5	Lattice Vibrations	11
3.6	Temperature Diffuse Scattering	12
3.7	First and Second Order Scattering	16
3.8	Effect of Anharmonicity on Phonon Interactions	17
3.9	Spatial Distribution of Temperature Diffuse Scattering	18
3.10	Instability and Lattice Dynamics	19
3.11	Models for Instability Analysis (a) Model of Woods, Cochran and Brockhouse	20
	(b) Model of Hardy and Karo	21
	(c) Modified Model of Hardy and Karo	22
CHAPTER IV	Experimental	
4.1	Alloy Preparation	27
4.2	Heat Treatment	28

	Subject	Page
CHAPTER IV		
4.3	Thin film preparation	28
4.4	Electron Microscopy and Diffraction	29
	(a) Hot Stage Microscopy	30
	(b) Dark field Microscopy	30
4.5	Volumetric Measurements	31
4.6	Single Crystal Preparation	31
4.7	X-Ray Intensity Measurements	31
CHAPTER V	Results and Discussion	
5.1	Pre-transformation (parent phase) Observations	32
	(a) Importance of Oxygen	32
	(b) Electron Microscopy and Diffraction	34
5.2	Nature of Thermal Diffuse Scattering	36
	(a) Direction of Streaking	37
	(b) Temperature Dependence of Length of Streaks	38
	(c) Confirmatory Observations	38
5.3	Instability in the Lattice of Parent Phase	41
5.4	Mode of "Freezing"	42
5.5	The Transition Phase (Dark Field Microscopy)	46
CHAPTER VI	Conclusions	50
CHAPTER VII	Suggestions for Future Work	52
APPENDIX A	Volumetric Measurements	53
APPENDIX B	Preparation of Single Crystals of TiNi	56

Subject		Page
APPENDIX E	X-Ray Intensity Measurements	59
TABLES		62
REFERENCES		65

LIST OF TABLES

Table	Contents
1	Composition of alloys and heat treatment schedule.
2	Calculation of intensity of Bragg reflections in x-ray powder patterns of TiNi.
3	Calculation of r.m.s. displacements from I_{TDS}.

LIST OF ILLUSTRATIONS

Figure	Subject
1	Specific heat of Barium Titanate (after Tisza, 15).
2	Satellites of the lattice point R_{hkl} corresponding to the wave whose propagation vector is $\vec{k}$. The first Brillouin zone surrounding R_{hkl} is shown with a dashed line (after Guinier, 17)
3 (a) and (b)	First and Second Order scattering.
4 (a) and (b)	Planar and Linear disorders (after Guinier, 17).
5	Model for the configuration of a negative ion and its nearest neighbours in a NaCl structure. D represents the regions of maximum displaced charge density (after Hardy, 26(i).
6.	Schematic model for positions of exchange charges about a central negative ion in an unstrained lattice. Large and small spheres are negative and positive ions, filled small black circles are exchange charges (after Dick, 29).
7	A pair of second nearest neighbour positive ions with their associated exchange charges indicated by small filled circles. The charge on B is modified due to the interaction of α and β with A. (after Dick, 29)
8	A pair of fourth nearest neighbours with associated exchange charges indicated by small filled circles. The charge on C is modified due to interaction of γ with A. (after Dick, 29)
9 (a) and (b)	Dispersion curves for the NaCl phase of RbI at the transition pressure (after Hardy and Karo, 28)
10 (a),(b) and (c)	Schematic representation of "satellites" and extra spots in the electron diffraction patterns observed in thermal cycling of TiNi thin films. (a) spots "A", "A_1" and "A_2" in the "quadrants" of (110) pattern, (b) spots "B" in (110) pattern, (c) setellites "C" in (111) pattern.
11 (a) to (f)	A series of (110) electron diffraction patterns from TiNi thin films observed at (a) 120°C, (b) 100°C, (c) 80°C, (d) 60°C, (e) near room temperature, (f) room temperature (with a slight tilt).

Figure	Subject
12 (a) to (e)	A series of (111) electron diffraction patterns from TiNi thin films observed at (a) 100°C, (b) 60°C, (c) 40°C, (d) near room temperature (e) on further cooling.
13	An example of streaks in (111) electron diffraction pattern, observed near the edge of a thin film.
14 (a) to (e)	A sequence of electron diffraction patterns showing streaks in (111) pattern observed on gradual tilting of the plane of diffraction about a {110} axis towards a (110) plane of diffraction.
15 (a) and (b)	Temperature dependence of the length of streaks. Appearance of "A" spots (schematic).
16	Temperature dependence of the length of streaks. Appearance of "C" spots (schematic).
17	Suggested behaviour of the "acoustic" dispersion curves with decreasing temperature, for the parent CsCl lattice of TiNi.
18 (a) and (b)	Suggested mode of distortion of parent phase lattice (a) in a (010) plane (b) in three dimensions, with resolved components shown by filled arrows. The components are associated with two transverse acoustic modes (or "phonons") of vibration, having wave lengths $2d_{001}$ and $2d_{110}$ respectively.
19	Definition of deviation parameter "S" (after Hirsch et al., 31).
20	Definition of beam divergence "α" (after Hirsch, et al., 31)
21	Dark field micrograph of the transition phase, x 20,000.
22	Dark field micrograph of the transition phase, x 20,000.
23	Dark field micrograph of the transition phase, x 60,000 (same area as figure 22).
24	Dark field micrograph of the transition phase, x 20,000
25	Dark field micrograph of the transition phase, x 40,000
26	Mercury dilatometer for volumetric measurements.
27	Volume changes on heating and cooling a 50 at.% Ni alloy.

CHAPTER I

INTRODUCTION

The near-stoichiometric composition region of the Ti-Ni phase diagram has drawn considerable interest in the past few years. Various investigators (1-9) have tried to understand the structure and phase transformations occurring in this intermetallic compound. Despite the contradictory findings of these investigators, it is generally agreed that the compound undergoes two phase transformations in the temperature range 700°C to room temperature. The upper transformation takes place at 600-700°C, and is of order-disorder type. The compound forms a CsCl type lattice at this temperature on cooling, with a lattice parameter $a_o = 3.01\text{Å}$.

It is, however, the low temperature transformation(s) that has aroused the most interest and controversy in the past few years. Some suspect this transformation to be of first order type, while others have suggested it to be of a diffusionless, second order type. With a greater understanding of analogous diffusional transformations, such as spinodal decomposition, and increased application of transmission electron microscopy, a more detailed picture of these low temperature transformations is beginning to form. This will become evident from the results of this investigation which was primarily designed to get a better understanding of the pre-transformation phenomena and the nature of the "transition" phase that forms as a result of a diffusionless, second order transformation prior to formation of martensite. A model for this parent-transition phase transformation is suggested based on lattice dynamics.

CHAPTER II

LITERATURE REVIEW

The low temperature phase transformations in TiNi have been investigated by various workers without much agreement in their results. Some have claimed no phase change (10) while others claim a room temperature phase transformation into a new structural phase or phases.

Purdy and Parr (3) first suggested that the intermetallic compound TiNi underwent a diffusionless, reversible transformation into a "π" phase near room temperature. This "π" phase was tentatively indexed as hexagonal with lattice constants $a_o = 4.572\mathring{A}$, $C_o = 4.660\mathring{A}$, $c/a = 1.02$.

In a series of papers, Buehler and his associates (4-6) have suggested that the parent CsCl structure of the compound undergoes a diffusionless transformation below 40°C in two stages, giving "TiNi II" and "TiNi III" phases, both of which could exist in equilibrium with the ordered "TiNi I" phase. Extensive x-ray diffraction work by Buehlar, Wang and Pickart (6) suggested this "TiNi II" phase to be of cubic type with a lattice parameter exactly three times that of the higher temperature "TiNi I" phase. This phase was found to form as a result of a "martensitic, pseudo-order-disorder" transformation at nearly 40°C. It was found to be unstable at lower temperatures, and a new phase "TiNi III" was formed, having a tetragonal lattice ($a_o = b_o = 9.0\mathring{A}$, $C_o = 3.0\mathring{A}$). Both these phases were found to be stable on heating up to nearly 350°C, and the formation of "TiNi III" phase was shown to be accompanied by several characteristics of a martensitic transformation. The zero-layer Buerger

(precession) x-ray photographs showed the existence of "TiNi II" and "TiNi III" as sets of streaks in the b.c.c. "TiNi I" diffraction pattern, even at 250°C. The lower temperature x-ray patterns showed the appearance of prominant superlattice of "TiNi II" at nearly 40°C, and then the "TiNi III" phase at 25°C. Their studies indicate a combination of replacement and displacement disorder associated with the 40°C transformation, and a second-order diffusionless transition is implied, even though it has not been claimed by them. These authors have failed to recognize that a single crystal need not remain a single crystal on transformatio

Dautovich and Purdy (7) studied the low temperature phase transformations in TiNi with the help of x-ray and electron diffraction, and resistivity methods. Their work indicated a transformation sequence: bcc (CsCl) parent phase→rhombohedral transition phase → triclinic martensite. The transition phase was shown to form as a result of a "second order" transformation mechanism by gradual distortion of the cubic lattice. The resulting unit cell had lattice constants of a_o = 6.02Å, and a maximum α = 90.7°. The formation of this rhombohedral phase was accompanied by a "doubling" of "{110} repeat distance" in electron diffraction patterns and splitting of diffraction maxima in x-ray powder patterns. The resistivity vs. temperature curve showed a gradual rise in this temperature region on cooling, before dropping suddenly at about 20°C due to formation of a martensitic phase. The martensite was labelled as triclinic with cell constants a_o = 4.60Å, b_o = 2.86Å, C_o = 4.11Å, α = 90.1°, β = 90.9°, and γ = 96.7°.

The selected area electron diffraction patterns of a 51 at. % Ni alloy, annealed at 500°C, taken at near room temperature showed some extra spots and a "tripling" of the "{110} cubic repeat distance", at places. This was tentatively attributed to the ordering of substitutional

defects associated with the increased deviation from stoichiometry due to precipitation of Ti_2Ni phase in the matrix. No corresponding changes were observed in x-ray powder patterns at the same temperature.

Elastic modulus studies of Wasikewski (8) have led him to conclude that the martensitic transformation in TiNi was of a "first order" type. The phase transformation was shown to be accompanied by a very low elastic modulus value at the transition temperature. The elastic behaviour of TiNi over a range of temperatures suggested an instability of the parent CsCl structure.

CHAPTER III

Theory of Second Order Transformations and Thermal Diffuse Scattering

3.1 INTRODUCTION - Transformation Types and their Speeds

Buerger (11) has classified the various types of transformations based on the change in bonding involved and associated coordination changes. From this point of view, the transformations can be categorised as:

1. Transformations of Secondary Coordination
   (or Network Transformations)
   (a) Displacive (rapid)
   (b) Reconstructive (sluggish)
2. Transformations of Order
   (a) Rotational (rapid)
   (b) Substitutional (sluggish)
3. Transformations of First Coordination
   (a) Dilatational (rapid)
   (b) Reconstructive (sluggish)
4. Transformations of bond type (usually sluggish)

The energy changes associated with a transformation correspond to a change in bonding of the atoms in the structure. Structurally, this means either an increase or a reduction in the interaction between neighbouring atoms - both near and distant neighbours. Thus, any change in the number and coordination, or arrangement of the neighbouring atoms, affects the crystal structure.

Our primary interest lies in the transformations of Secondary Coordination type which are displacive in nature. These displacive transformations do not involve any change in the first coordination of the atoms, and any change is associated with a change in non-nearest neighbour bonds. Such energy changes are small. Changes in secondary coordination can take place by either a breaking and subsequent restoration of a network (reconstructive type), or simply by a continuous displacement of atoms without any break in linkage. The structure becomes distorted so that non-contacting atoms are displaced with respect to one another. In this type of transformation the parent structure is an "open", low coordination one that "collapses" into one of lower symmetry (and lower entropy) on cooling. No energy barriers exist for such a kind of distortion. These transformations are therefore, very rapid in speed.

An example of such a displacive transformation is provided by Barium Titanate (12) that transforms from cubic into a tetragonal form on cooling.

Thermodynamically, all the above types of transformations can be classified into two kinds: (a) First Order type, in which energy, volume and crystal structure change discontinuously, and (b) Second Order type, in which energy and volume change continuously, but the temperature derivative of these quantities have singularities at the transition point.

3.2 Landau's Theory of Second Order Transitions

Ehrenfest (13) has defined a transformation of nth order as the one in which the first discontinuity of the derivative of free energy with respect to temperature and pressure occurs in the nth derivative.

According to Landau (14), the First Order transformations can be explained satisfactorily by the phase theory of Gibbs, with experimental evidence supplementing more specific information. Most diffusionless transformations are of this type. A sudden change in symmetry is usually observed in these transformations, with the two phases of different symmetries existing in equilibrium at the transition point.

The Second Order transformations are, however, not so explicit thermodynamically. Diverse molecular mechanisms underlying this type of phase change may have similar thermodynamic features. In this type of transformations, a "curie point" or "λ-point" exists, on either side of which the lattice differs only slightly. But an abrupt change in symmetry may still be presumed over an infinitesimal period at the Curie point. A number of symmetry elements appear or disappear abruptly at a "λ-point".

No abrupt change in probability distribution of atoms in the lattice is observed, even though the lattice suddenly acquires a new symmetry at a "λ-point". The new lattice is usually of a lower symmetry.

Quantitatively, the changes at a "λ-point" can be described through a variable η, which is a measure of deviation between the two states existing on either side of the "λ-point". This variable vanishes for the state of higher symmetry and has a finite non-zero value for the lower symmetry state. Thus, near the "λ-point", G(p, T, η), the Gibbs free energy may be expressed as:

$$G(p, T, \eta) = G_0 + G_1\eta + G_2\eta^2 + \ldots \qquad (1)$$

It can be shown from this equation that at the actual "λ-point",

the following relation must be satisfied for minimum G:

$$\left.\frac{\partial^2 G}{\partial \eta^2}\right|_{\eta=0} = 0 \qquad (2)$$

This derivative is < 0 for the state with lower symmetry, and is > 0 for the higher symmetry state.

This indicates that entropy remains continuous through the "λ-point" and so are volume and energy of the system. The specific heat Cp has a finite jump ΔCp at the "λ-point" as shown in figure 1. It is found to increase in the transition from the more to a less symmetrical state. Similar jumps are observed in Cv, compressibility $-\frac{1}{V}(\frac{\partial V}{\partial p})_T$, and thermal expansion $\frac{1}{V}(\frac{\partial V}{\partial T})_p$.

3.3 Tisza's Theory of Second Order Transitions

Onsager's calculations based on the Ising model show that there is a logarithmic infinity in specific heat Cp at the "λ-point". Such a prediction called for a moderation of Landau's theory, which predicts a finite jump in Cp at the transition point, and Tisza (15) has attempted to clarify this difficulty in his theory.

For a homogeneous system, the intrinsic properties of the system, such as stability, internal energy U, etc. can be expressed as a function of γ independent variables in the form:

$$u = u\,(x_1, x_2, x_3 \ldots\ldots x_\gamma) \qquad (3)$$

For each value of x_i, we have:

$$Pi = \frac{\partial u}{\partial x_i} = \text{force or pressure.}$$

For a stable equilibrium, the forces $P_1^{(o)}, P_2^{(o)} \ldots P_\gamma^{(o)}$

should be balanced by equal and opposite external forces. The equilibrium is stable, if:

$$\delta^2 u = \frac{1}{2} \sum_{1}^{\gamma} u_{ik}\, \delta x_i\, \delta x_k > 0 \tag{4a}$$

This quadratic form can be transformed into the form:

$$\delta^2 u = \frac{1}{2} \sum \lambda_k\, \eta^2_k \tag{4b}$$

by a non-singular linear transformation with

$$\lambda_k = \frac{\partial^2 u\,(P_1, P_2 \ldots P_{k-1})}{\partial x^2_k} = \left(\frac{\partial P_k}{\partial x_k}\right)_{P_1, P_2 \ldots P_{k-1}} \tag{5}$$

At a λ-point, or Critical point, one of the λ_k coefficients vanishes. This predicts a vanishing of the determinant D_γ at the critical point, where D_γ is given by:

$$D_\gamma = \begin{vmatrix} u_{11} & \ldots\ldots\ldots & u_{1\gamma} \\ & \ldots\ldots\ldots & \\ u_{\gamma 1} & \ldots\ldots\ldots & u_{\gamma\gamma} \end{vmatrix} = \lambda_1\, \lambda_2 \ldots \lambda_\gamma \tag{6}$$

Thus, coefficients like

$$\upsilon_{ik} = \frac{U_{ik}}{D_\gamma} \qquad (U_{ik} \text{ being co-factor of matrix element } u_{ik})$$

tend to become infinite at transition points, unless U_{ik} also vanishes. Thus, singularities are predicted in the usual thermodynamic formalism.

However, since the thermodynamic theory fails at the critical point, it can only be stated that the coefficients υ_{ik} have unusually large values when approaching a critical point. The exact nature and

degree of this singularity can only be predicted by a rigorous statistical calculation. By choosing proper variables, like pressure, temperature, entropy, etc., it can be shown that at the critical point infinite values are expected for coefficients like dielectric constant, specific heats Cp and Cv, compressibility, etc. Any reduction in the number, or a wrong choice of relevant variables, will lead to a "λ-anamoly" in specific heat, of the kind shown in Landau's theory.

The above theory, however, does not say anything about the molecular mechanisms involved and is a very general one. It holds well for most "displacive" transformations in Buerger's terminology.

3.4 Quasi-Thermodynamic Formalism of Tisza and Klein

For systems where a purely thermodynamic theory fails to explain the critical points, a quasi-thermodynamic model is proposed by Tisza and Klein (15).

They divided a system into N equal cells, each having coordinates, or quantam numbers Z_1, Z_2, Z_3 ... Z_ν. The whole system thus has N.ν parameters for specification. These parameters can be chosen in the form of normal coordinates having definite phase differences for neighbouring cells. Such a phase difference may be taken as "zero" (or infinite wave length). These parameters also include additive integrals of motion, atomic parameters specifying the equilibrium positions of the atoms in the unit cell, etc. It is seen that macroparameters, such as the last named, give rise to coherent x-ray or electron scattering, and the corresponding statistical parameters like lattice vibrations or "phonons" give rise to diffuse scattering. No conjugate forces (as is the case with purely thermodynamic parameters) are associated with quasi-thermodynamic

parameters as explained on the previous page.

Such a theory leads to a similar condition, as predicted by Landau in his quasi-thermodynamic theory, for the critical point, i.e.

$$\lambda_3 = \frac{\partial^2 u\,(T,P)}{\partial \eta^2} = \frac{\partial^2 g}{\partial \eta^2} = 0 \qquad (7)$$

where

$$u\,(T,P) = g = u - Ts + Pv$$

is the Gibbs function per mole.

Landau computed the specific heat and predicted a definite increase ΔCp in specific heat in going from a state of higher symmetry to one of lower symmetry. Tisza and Klein, on the other hand, predict an infinite singular value for Cp at the critical point as a result of the "interaction" of thermodynamic parameters, which Landau overlooked.

3.5 Lattice Vibrations

The nodes of a regular lattice are positions of equilibrium around which the atoms vibrate. The frequency of vibration of atoms is small compared to that of x-rays or electron beam. The amplitude of vibration increases with temperature.

Debye (16) first suggested that the thermal energy of the solid is distributed amongst the normal modes of vibration of the crystal. He proposed that these atomic vibrations were independent, resulting in a diffuse scattering spherically symmetrical in reciprocal space. Laval, however, showed for the first time that the diffuse scattering of x-rays in reciprocal space was highly anisotropic. The hypothesis that atomic vibrations are independent must, therefore, be rejected. A critical

analysis of thermal vibrations by various workers, indicated that the displacement of atoms acted on one another.

Born and Huang (16) have suggested that these vibrations of atoms could be considered to be the superposition of displacement waves propagating through the crystal lattice. These lattice waves are coupled together due to anharmonicity. Anharmonicities arise from third and higher order terms in the potential energy of a displaced atom. The part played by these terms is analogous to that of collisions in the theory of a perfect gas. Though introducing only a small perturbation of motion, they are responsible for the coupling of the normal modes, which is essential for thermal equilibrium. Peierl's theory of heat conductivity of crystals shows that these normal modes of vibration of a crystal lattice are quantized, the quanta of vibrational energy being termed "phonons".

Each normal mode, conventionally represented as a standing wave, may be analyzed into travelling waves in opposite directions. Each wave produces its own diffraction effect.

3.6 Temperature Diffuse Scattering

Any perturbation in the crystal lattice results in a diffracted radiation which is not well localized, in contrast to that expected from a perfect crystal. The average ideal lattice, however, still gives strong diffracted radiations at angles satisfying Bragg's Law, but in other directions the wavelets emitted by the individual atoms do not perfectly cancel each other by interference because cancellation is a direct consequence of the perfect periodicity of the diffracting lattice.

This effect is called "Diffuse scattering". The total diffracted intensity $I_{(\vec{s})}$ is given by:

$$I_{(\vec{s})} = I_1(\vec{s}) + I_2(\vec{s}) \tag{8}$$

where $I_1(\vec{s})$ represents that part of diffracted radiation that comes from a perfect crystal with average structure factor $\overline{F}$. $I_2(\vec{s})$ is the intensity of diffuse scattering given by the expression:

$$I_2(\vec{s}) = \sum_m V(\vec{x_m}) \quad \phi_m \exp.(2\pi i \vec{s}\, \vec{x_m}) \tag{9}$$

This contains a shape factor and a "correlation function" ϕ_m that measures the correlation of perturbation from one unit cell to another.

If the correlations are not strong, ϕ_m tends to zero, and for strong correlations ϕ_m approaches unity.

(a) If there is no correlation, only ϕ_o is different from zero, and ϕ_m is represented by a $\delta(x)$ function whose transform is constant. The total diffuse scattering is given by:

$$I_2(\vec{s}) = \left|\overline{F}_n\right|^2 - \left|\overline{F}\right|^2 \tag{10}$$

which is independent of $(\vec{s})$. In this expression $\left|\overline{F}\right|$ is the average structure factor of the real crystal. A general background of uniform intensity will be observed in this case.

(b) If there is a strong correlation, $(\phi_m \neq 0)$, ϕ_m decreases slowly with m and the diffuse scattering is concentrated around the reciprocal lattice modes.

(c) If ϕ_m is periodic, and has a form of a plane wave proportional

to cos $(2\pi \vec{k}.\ \vec{x}_m)$, the diffuse scattering is concentrated at two points which are symmetrical about the nodes of the reciprocal lattice at the distance $\pm$ k, where $\vec{k}$ is the "propagation vector" for the perturbation $(|\vec{k}| = \frac{1}{\lambda})$. For all other regions of the reciprocal space the summation for $I_2(\vec{s})$ is zero.

With this brief discussion of the nature of diffuse scattering, the particular case of thermal or "temperature diffuse scattering" will now be discussed.

In addition to the incoherent diffuse scattering of x-rays and electron beam by a perturbed lattice, there is a coherently diffracted or "reflected" radiation which is scattered by interaction with the above mentioned "phonon" waves. The existence of this phenomenon was first suggested by Faxen and Waller (17). According to this theory, the regular periodicity of a crystal lattice is disturbed by each phonon wave, giving rise to a series of dynamic stratifications corresponding to each set of static lattice planes. These dynamic stratifications are inclined at small angles to their associated lattice planes. It is thus possible to get a coherent reflection from these dynamic stratifications, but at angles not satisfying the Bragg condition with respect to the static lattice planes. The strength of this reflection will depend on the amplitude of modulation, i.e. the amplitude of the phonon wave. The latter is again dependent on frequency of the wave, owing to the partition of energy along the different modes of vibration. The amplitude of the wave is related to the velocity by the relation:

$$A_i^2 = \frac{2kT}{\nu_i^2} = 2\ kT\ (\frac{\lambda_i}{u_i})^2 = \frac{E_{\nu_i}}{2\pi^2\ Nm\ \nu_i^2} \qquad (11)$$

k being the Boltzmann's constant, m is the mass of the atom, u_i and v_i are the velocity and frequency of the ith wave respectively.

It is obvious, on general grounds, that for small amplitudes, the greater the amplitude of the wave perturbing the lattice, the greater is the amplitude, and thus the intensity, of the corresponding scattered ray.

Consider the lattice to be consisting of N atoms in a volume V, so that there are 3N waves traversing through it. The displacement of an atom situated at node $\vec{x}_n$ may be represented by:

$$\Delta \vec{x}_n = \vec{A} \cos 2\pi (\nu t - \vec{k}.\vec{x}_n) \qquad (12)$$

where ν and $\vec{A}$ are the frequency and amplitude of oscillation of the atom. The vibrations are in phase at nodes, which satisfy $\vec{k}.\vec{x}_n$ = constant.

The vector, $\vec{k}$, or the "propagation vector" is normal to the wave fronts, and is related to the wavelength by the relation:

$$\lambda = \frac{1}{|\vec{k}|}$$

Since the frequency of vibration of atoms is small compared to that of x-rays or an electron beam, the atoms may be assumed to occupy fixed positions on a diffraction grating for calculation of scattering intensity, with displacement defined by the vector:

$$\Delta \vec{x}_n = \vec{A} \cos (2\pi \vec{k}.\vec{x}_n) \qquad (13)$$

The coefficient ϕ_m is given by, in this case:

$$\phi_m = 2\pi^2 f^2 (As \cos \alpha)^{\frac{1}{2}} \cos [2\pi \vec{k}\,\vec{x}_m] \qquad (14)$$

where f is the average structure factor and α is the angle between vectors $\vec{A}$ and $\vec{s}$.

It can be shown, as before, that for a periodic ϕ_m, with a sinusoidal variation with vector $\vec{k}$, the scattered intensity is concentrated at two points at distances $\pm \vec{k}$ from the nodes of the reciprocal space. The intensity of these two "satellite" points is equal to the loss in intensity of Bragg reflections.

The satellites (fig. 2) may be assumed to be Bragg reflections from a series of equidistant planes which are normal to the vector $\overrightarrow{OP}$, joining the origin to the satellite in reciprocal space, with a spacing $\lambda = \frac{1}{OP}$. These planes lie on a wave front with propagation vector $\overrightarrow{OP}$. This corresponds to the same wave which has a propagation vector $\overrightarrow{R_{hkl}P}$.

The set of the smaller, or the "fundamental propagation vectors" e.g. $\overrightarrow{R_{hkl}P}$, around a given node lie within a region defined by the first Brillouin zone, as shown in figure 2.

3.7 <u>First and Second Order Scattering</u>

The intensity of the diffusely reflected wave at a particular setting can be considered to be made up of different components, called "First Order", "Second Order", etc., according as it has interacted with one, two or more thermal waves. The intensity of diffuse reflections decreases with increasing order of reflections.

Laval (18) has shown that the first order diffuse reflection at an element of reciprocal space around a point P is produced by elastic waves having their wave vector $\vec{k}$ equal to $\pm$ QP, where Q is the reciprocal lattice point ("relp") nearest to P (figure 3a).

Similarily, the second order diffuse reflection (figure 3b) from P is produced only by the combined action of pairs of waves, the wave vectors $\vec{k}_i$ and $\vec{k}_j$ of which add vectorially to $\pm$ QP as shown.

For a given wave vector $\vec{k}$, there are, in general, in the lattice a number of waves with different frequencies which may be classified as "acoustical" and "optical" waves. The former have a low frequency and long wave length, while the latter have relatively high frequencies and are therefore much less effective in producing diffuse reflections owing to their small amplitude.

At long wave lengths, atoms of a unit cell move as a whole, in phase, in case of "acoustic" modes, whereas they move with respect to each other in the case of "optical" modes. The frequency of acoustical waves tends to zero as wavelength tends to infinity, while that of optical waves approaches a finite value (optical range). Usually, therefore, the effect of optical modes is neglected, so far as diffuse scattering of electron beam or x-rays is concerned.

3.3 Effect of Anharmonicity on Phonon interactions

Suppose that a disturbance of wave vector $\vec{k}$ moves through a solid. As the lattice vibrates some atoms come closer than their equilibrium distance, others move farther apart. Another phonon, of wave vector $\vec{k}'$, attempting to pass through the medium, will see the elastic properties slightly altered. Where the lattice is compressed, the effective elasticity will be changed because of the anharmonicity of the interatomic forces (19). The phonon $\vec{k}$ will thus generate a periodic variation in the refractive index of the medium, and the phonon $\vec{k}'$ will be reflected from this, as if from a diffraction grating. With this grating moving, one would expect a complicated interference effect, but it can be shown that the reflected phonon will have a wave vector $\vec{k}''$ given by:

$$\vec{k}'' = \vec{k} + \vec{k}' \qquad (15)$$

In a continuous medium, this sort of scattering is always possible - but in a lattice there is a rule that no wave vector may be so large as to lie outside the first Brillouin zone. If $\vec{k}$ and $\vec{k'}$ are so large as to make this so, even then such a scattering process is possible (defined by equation 15) - as a vibration of such short wave length as a lattice wave may be considered as a much longer wave length vibration. On the left hand side of equation 15 we put $\vec{k''} + \vec{g}$, and say that $\vec{k''}$ is the "real" vector of the reflected phonon. It is obvious from the definition of Brillouin zone and the reciprocal lattice that there is only one value of $\vec{g}$ which brings $\vec{k''}$ inside the first zone.

3.9 Spatial Distribution of Temperature Diffuse Scattering

Thermal agitation of crystals, discussed above, is an example of "displacement disorder" (17) in which the atoms are displaced from their equilibrium position momentarily by distances small compared to interatomic distances. Long range order is still preserved in this case. As explained earlier in section 3.6, the distribution of diffuse scattering in reciprocal space is a function of the degree of correlation between the perturbations travelling in various directions.

Such disorder can be either "planar" or "linear". In planar disorder, a family of planes preserves its periodicity over the lattice, though they are no longer arranged regularily. Such a situation arises when the planes are displaced parallel to themselves in irregular manner. In such a case, the scattering is limited to the rows of the reciprocal lattice which are normal to the lattice planes whose structure is intact.

The reciprocal equivalent of a single plane of atoms arranged on a regular net is a series of diffuse rods which are all normal to the

plane of atoms. The diffuse rods pass through the nodes of reciprocal lattice corresponding to the atomic distribution in actual lattice. This is shown clearly in figure (4a).

In linear disorder, the periodicity of the lattice is preserved in only one direction. The parallel rows of atoms are periodic, but not arranged regularily. A row of equally spaced atoms has a reciprocal equivalent of a series of diffusely reflecting equally spaced planes which are perpendicular to the row of atoms. The interplanar distance is inverse of the distance between successive atoms in the rows. This is illustrated in figure (4b).

Thus, a disc of disturbed region of the lattice produces a diffuse "streak" or "rel rod" normal to the plane of the disc passing through each reciprocal lattice point. A rod of disturbed crystal lattice, conversely, produces a disc of diffuse reflections around each reciprocal lattice point.

3.10 Instability and Lattice Dynamics

A thermodynamic analysis of the displacive phase transformation of the kind observed in TiNi does not give any indication of the nature of the instability involved in the system. This instability is analogous to the one observed in the case of spinodal decomposition. Cahn (20) has shown that if a metastable phase is unstable to infinitesimal composition fluctuation, then there is no barrier other than a diffusional one, for it to transform continuously ("second order") to a more stable phase. This diffusional decomposition is called "spinodal decomposition". Contrary to this, the diffusionless second-order transformations are associated with a mechanical instability.

In recent years, the problem of crystal stability and second order transitions has been recognised as one involving lattice dynamics. Mechanical instability involved in such systems has been discussed at length by Born and Huang (16) and a theory has been proposed by them based on lattice vibrations. They have proposed that for a crystal to be stable for all small deformations, all the normal modes of vibrations of its lattice should have real frequencies. Instability is introduced in the crystal when any of its normal modes of vibration approaches zero frequency. A unique identification of such a mode depends largely on the model chosen for the crystal atoms or "ions", as will become evident in the following section.

3.11 Models for Instability Analysis

(a) Model of Woods, Cochran and Brockhouse

In the general theory of lattice dynamics of alkali halide crystals, which is applicable to all dioatomic crystals having tetrahedral symmetry around each ion (e.g. NaCl, CsCl, ZnS and isomorphous structures) Woods, Cochran and Brockhouse (21) have shown that instability can set in when some of the acoustic frequencies become imaginary. Their approach is based on the "shell model" of ionic crystals used by Lyddane and Herzfeld (22), Hanlon and Lawson (23) and Dick and Overhauser (24) - with certain "extensions". The instability, with respect to acoustic frequencies, is sensitive to these "extensions", in that the distortion polarization of the ions is neglected. The polarization is assumed to depend only on the electric field about the ion and not on the distortion of ions. These authors point out that this seems highly unlikely in actual crystals, as will become clear in the following section.

In a study of ferroelectric crystals, Cochran (25), using the same model as above, has suggested that in ferroelectric transitions in simple diatomic cubic crystals, instability is associated with the transverse optic mode of vibration approaching zero frequency. The crystal remains stable against other vibrational modes. The use of "shell model", however, introduces certain constraints in the calculation of the effect of the distortion polarization. Such constraints have been removed in the model selected by Hardy and Karo (26).

(b) Model of Hardy and Karo

In their study of the lattice dynamics of NaCl type structures, Hardy and Karo (26) have calculated the dipole moment on a given ion in a way which allows not only for its displacement as a point charge, but also for the distortion introduced in the electronic charge distribution. This is regarded as consisting of two parts:

(i) A component of $\pm e_{eff}$ arising from the displacement of the ion as a rigid point charge.

(ii) A component due to the distortion of the electronic charge distribution in the perturbed lattice.

Szigeti (27) was first to show the effect of short range polarization associated with "overlap" repulsion due to (ii). The effect of this overlap is to redistribute the charge in the regions of overlap which results in a separate contribution to the dipole moment. This is additional to the polarization due to the effective electrostatic field, and would be present even if the lattice were composed of "atoms" instead of ions.

In the model of Hardy and Karo, the electronic configuration of a negative ion and its six nearest neighbours is as shown in Figure 5 for a NaCl structure.

The charge density in the crystal is shown to consist of spherically symmetrical negative components centred on each ion, together with a positive contribution D which produces an overall cubic symmetry.

In the undistorted lattice, the neutrality of the crystal is maintained, but in a uniformly polarized crystal (or a perturbed lattice) this is no longer true. A dipole moment, linear in the relative displacement of the two sub-lattices is present.

The higher order multipole effects are neglected in their calculations, as the parameters involved are complex and impossible to calculate.

(c) Modified Model of Hardy and Karo

The modified model of Hardy and Karo (28) includes second neighbour interactions and long range interatomic forces (or "three body" forces). These long range forces are represented by classical multipole interactions, the dipolar term being most prominant.

The model chosen for this approach is the one used by Dick (29) in his theory for ionic crystals. The repulsion of ions is possible only when they overlap. In the region of overlap, schematically represented in the figure 6, Pauli's exclusion principle acts to reduce the electron charge density and to distribute the reduced charge in spherical symmetry about the ions. The regions of reduced charge may be taken as superposed positive charge; localized between neighbouring ions. This superposed charge is called "exchange charge" and these charges are located symmetrically in an unstrained crystal. But when the crystal is strained or

distorted, the magnitude and position of these charges is changed. Since the position and magnitude of the exchange charges depends on the positions of the ions nearest to these charges, the interaction of two exchange charges with one another depends on the positions of the four neighbouring ions. Thus, exchange charge interactions have a "many body" nature. This is illustrated in the figures 7 and 8 for second and fourth nearest neighbour interactions.

The dipole moment on any given ion is taken to consist of two independent components - one induced by the local electric field, and the other due to the distortion of the electron cloud between first nearest neighbours by "overlap". The effect of overlap, as explained above, is represented by a localized charge in each bond, which again is compensated by a uniform change in the free ion distributions. Assuming this localized distortion as being associated with the positive ion, the monopole moment at a given site k is changed from $\pm$ e to

$$e_k = \pm e \left[1 + \sum f(\gamma_i)\right] \tag{16}$$

where k = 1 for positive ions, and 2 for negative ions. The sum is taken over 6N.N first nearest neighbours, γ_i being the respective distances from the central ion.

$$\text{Thus, } e_1 = e\,(1 + 6f)\ ,\ f = f(\gamma_o) \tag{17}$$

The cohesive energy, calculated from equation (16) by determining individual terms in equation 17, involves "3-body terms" which are responsible for the deviation from Cauchy's relationship $C_{12} = C_{44}$ for cubic crystals. The total cohesive energy U is given by:

$$U = U_{SR} + U_{++} + U_{--} + U_{+-} \tag{18}$$

U_{SR} is the short range repulsive term introduced on considering the overlap. It is given by:

(19)

where ρ is density of the material.

A detailed analysis of equations 16 and 18 leads to the deviation:

$$C_{12} - C_{44} = \frac{2.3301\ e_1 e f'}{\gamma_o^3} \tag{20}$$

where

$$f' = \left.\frac{df(\gamma)}{d\gamma}\right|_{\gamma = \gamma_o} \tag{21}$$

Dispersion curves can be calculated for acoustic modes by using the relation:

(22)

where C is a linear combination of elastic constants C_{11}, C_{12}, C_{44}.

Knowing the elastic constants, f and f' can be calculated, when $f(\gamma)$ is taken as proportional to overlap.

The effect of overlap on e_k can be split into two parts:

(i) that arising from the relative motion of ions on the same sub-lattice.

(ii) that arising from the relative displacement of ions on two different sub-lattices.

Short wave length optic modes are less sensitive to the effect of overlap as one might expect the rapidly alternating signs of the dipoles

at the other ion sites to produce a large measure of concellation in their total interaction with the quadrapole moment on O in figure 5. Long wave length optic modes have no associated field gradient, therefore, the dipole quadrapole interaction vanishes.

From these considerations, it is evident that the relative size of this contribution to the second order terms in the expansion of lattice energy is likely to be largest for nearly uniform strains such as those associated with the long wave length acoustic modes, or whenever frequency tends to zero, where the distribution function $N(\nu)$ of frequencies is most sensitive to its presence. In case of long wave length acoustic modes, the contribution from (ii) is zero, whereas reverse is true for long wave-length optic modes.

Applying the above analysis to the particular case of RbI, Hardy and Karo have shown that the effect of the previously mentioned "3-body" forces figures prominantly in the analysis of instability of the NaCl phase. Neither second nearest neighbour interaction alone nor second neighbour interaction plus ionic deformation will result in crystal instability. It has been shown that the NaCl phase in the RbI crystal becomes unstable when the frequency of the transverse (and longitudinal) acoustic mode with a wave vector at the centre of the [100] zone face approaches zero frequency. The crystal is shown to become unstable with respect to a relative motion of the two sub-lattices along a <110> direction. This becomes apparent when the value of the elastic constant C_{12} is seen to become unusually large near transition point. Their dispersion curves for RbI are given in figure 9.

It becomes quite evident from above considerations that the explanation of instability from crystal dynamics point of view is very sensitive to the model selected for the crystal ions and the selection of the variables that have any effect on interatomic cohesive energy.

CHAPTER IV

EXPERIMENTAL

4.1 Alloy Preparation

Three compositions of alloys were used primarily for this investigation, containing 51 at.%Ni, 50.5 at.%Ni and 50.0 at.%Ni respectively. The alloys were prepared in ingot form using iodide titanium (99.92% pure) and standard spectrographic nickel (99.99% pure), by melting in argon arc melting furnace under gettered inert atmosphere. The loss in weight was calculated in each case and amounted to an average 0.015% of the total weight charged. Specimens were prepared for metallographic investigation to determine the presence of any second phase, and none was observed in any of these alloys.

Homogeniety of the final specimen was ensured by melting the button from both top and bottom alternately at least three times. Melts of weights ranging from 50 gm. to 75 gm. were normally prepared for ease in handling during further working of the ingot. The ingots obtained were of average diameter approximately 1/2".

The ingots so obtained were hot swaged and then made into thin sheet (∿ 0.004" thickness) form by a combination of hot and cold rolling. Frequent stress relieving while cold rolling was done by heating the thin sheets at one end for a short time. The sheets so obtained were mechanically polished to remove any oxide film at surface, before subjecting them to the heat treatment.

4.2 Heat Treatment

Though some thin films were prepared from as cast, and cold worked materials, most of the observations were made on annealed specimens. All the sheets annealed were first mechanically polished to remove any oxide layer and surface contaminations prior to heat treatment. The samples were then sealed in "vycor" tubes at nearly 10^{-6} mm Hg and annealed as per the schedule given in Table 1. No surface discolouration was detected after such treatments.

The alloy A-1* was taken in ingot form and machined down to ~1/2" diameter rod form before annealing. Thin sections (approx. 0.011" thickness) were cut from this rod with the help of a "Servomet" spark cutter for a strain free cut. The rest of the alloys were taken in sheet form for annealing.

4.3 Thin Film Preparation

Thin films for transmission electron microscopy and diffraction were prepared from the above mentioned sheet specimens by electro-polishing, using the "window technique". The initial electrolyte used had a composition of 59% Methanol, 35% Ethylene Glycol and 6% Perchloric acid. The "plateau" in current vs. voltage curve was observed at 24V, and a temperature of -10 to -20°C was found to give the best results. However, it was discovered, especially with cold worked sheets, that this electrolyte polished too fast and the thin films so obtained were not of a very good quality. A solution with 3% Perchloric acid, 62% Methanol and 35% Ethylene Glycol was found to yield better results under similar polishing conditions (24V, at nearly -30°C) and this electrolyte was used for all the present work. Stirring was required to avoid preferential attack away from the centre of the specimen.

The edges of the specimens (of approximate size 0.6 cm x 1 cm) were coated with microstop and manual stirring was applied. A U-shaped stainless steel cathode was used and the specimen waved back and forth between its edges. All the thin films so prepared were found to be martensitic, as expected.

4.4 Electron Microscopy and Diffraction

Small sections from the thin films prepared as explained in section 4.3 were put in a Seimens Electron Microscope and observed at 100 kv. The small thin sections were washed with acetone and ethanol before examination in the microscope. The fresh thin sections were invariably martensitic in structure, part of which reverted to a mixture of parent (bcc) and transition phases on heating the thin film by the electron beam itself (by removing the objective aperture) and allowing it to cool down.

The thin sections, when freshly prepared, showed some "cloud"-like waves moving across in all directions of the foil. The nature of these waves (which are distinctly different from dislocation movements) still remains to be explained, but it is suspected to be associated with the mechanical instability of the foil.

Due to the limited low temperature range of stability of the transition phase it was very difficult to catch the "doubling" spots of the "{110} repeat distance" in (111) diffraction pattern in fresh foils, and care was taken to have very little or no bias in the beam while studying it. It was also observed that such studies were best made on thin films with a coarse initial martensitic structure. This was achieved, in cases not already present, by allowing the foil to "age"

at room temperature for a few days.

(a) Hot Stage Microscopy

Thermal diffuse scattering observations were made using a "heating stage" in the object chamber of the microscope. The heating device was a non-tilting hot stage which allowed temperature control within $\pm$ 2°C. The thin foil was maintained at each temperature level of observation for at least 15 minutes to ensure uniform heating. The temperature range of working of this hot stage was up to 1000°C, but the thin sections used were never heated to more than 300°C to avoid excessive oxidation and contamination. However, some contamination of the foils was unavoidable each time the heating cycle was repeated, and fresh sections were used for each set of experiments. The cartridge used in these runs was a standard Platinum cartridge, and Molybdenum grids were used instead of the usual copper grids. The magnification in case of the micrographs taken with the heating stage was 85-90% of the normal magnification without one, due to the longer length of the cartridge. The condenser (C2) was over-focussed (rather than under-focussed) a few medium clicks to get a more unifrom illumination intensity, and to get sharply focussed spots in the diffraction patterns.

A standard calibration curve, provided by the manufacturers, was used to estimate the temperature of the specimen from the input wattage to the heating system of the hot stage. A d.c. supply source of 12V, 0.7 amp. was used for this unit.

(b) Dark field Microscopy

Dark field observations were initially made by putting the smallest objective aperture on the particular spot of interest in the

diffraction pattern, and projecting its image. These micrographs were found to be of poor contrast and low resolution. Better results were obtained by centering the spot of interest along the optical axis of the microscope by tilting the gun, and then projecting its image. This gave better resolution and a more uniform dark field image. The phase (or "phases") contributing to the particular spot in the diffraction pattern came up in "bright field" in these micrographs. A more detailed discussion on this work is presented in next chapter.

4.5 Volumetric Measurements

The volume changes accompanying the martensitic transformation were measured using a vacuum sealed mercury dilatometer and a "Haake Unitherm" temperature controlled bath. Details of these observations are given in Appendix A.

4.6 Single Crystal Preparation

Several attempts were made, using a variety of techniques to grow a single crystal of the intermetallic compound for a proposed ultrasonic study of elastic constants, all resulting in near failure. Details are discussed in Appendix B.

4.7 X-Ray Intensity Measurements

An analysis of the diffuse background in the x-ray powder patterns, and the intensity of parent CsCl Bragg reflections in powder patterns, was made by taking intensity charts on a photodensitometer (and diffractometer). The contribution of thermal diffuse scattering to the background, and the r.m.s. displacement of atoms in various directions were calculated under isotropic assumptions. Details are discussed in Appendix C.

CHAPTER V

RESULTS AND DISCUSSION

5.1 Pre-transformation (Parent Phase) Observations

The "displacive" nature of the bcc (CsCl) parent phase - rhombohedral transition led the present author to investigate the nature of structural changes leading to this instability.

Thin films prepared by electropolishing as rolled (cold worked), as cast and annealed specimens were first observed in the electron microscope at room temperature and were invariably found to be martensitic. This was expected, of course, as the polishing bath temperature was kept close to -30°C, which gave a high degree of supercooling with respect to the martensitic transition.

It was observed however, that the martensite partially reverted to the ordered bcc structure (parent phase) if the thin films were aged at room temperature for short times, or observed in the microscope. Such foils showed both bcc and rhombohedral diffraction patterns in most cases after this aging, but no complete reversion of martensite was ever observed as the reversion temperature was well above room temperature.

(a) Importance of Oxygen

The amount of oxygen as an interstitial impurity plays an important role in the martensitic transformation in TiNi. It is believed present mainly in the form of $Ti_4Ni_2O_x$, which has a tendency to precipitate

out as second phase on long isothermal treatments. Wasilewski (8) has shown that the amount of oxygen affects the reactions time. The hysteresis in the reversible martensitic transformation is increased by greater oxygen contents. For example, the hysteresis in an alloy with 480 ppm oxygen was more than 85°C compared to an average 25°C for alloys with a moderate oxygen content of 146 ppm.

Dautovich, et al (9) have shown that the martensitic reaction may be suppressed in low oxygen samples. No transformation was observed in highly pure alloys. Long isothermal anneals at 400°C resulted in samples containing less than 200 ppm oxygen and the transition phase was found to be stable over a considerable range of temperature in this alloy, thereby suppressing the martensitic transformation. Longer isothermal anneals, however, limited the temperature range of stability of transition phase, and the martensitic reaction was observed close to room temperature. This was believed to have been caused by the formation of a finely dispersed, coherent, impurity rich precipitate which reduced the oxygen content in the bcc TiNi phase.

The failure of some workers (10) to observe the martensitic transformation over a temperature range -20°C to 160°C probably may be attributed to a high oxygen content in the TiNi phase within the samples, which may have increased the hysteresis considerably.

Some of the alloys used in this investigation were analyzed for oxygen after treatment, and were found to contain approximately 112 ppm oxygen by weight. Thin films prepared from all the alloys listed in

Table 1 showed a completely martensitic structure when taken fresh out of the polishing bath. A complete reversibility in phase transformations was observed in all the samples.

(b) Electron Microscopy and Diffraction

A series of electron diffraction patterns were taken at various temperatures in the range 300°C - room temperature, on foils prepared from alloys listed in Table 1. The results obtained were the same in each case and will be discussed now.

The diffraction patterns taken on a fresh foil from alloy A-5, in the heating cycle (from room temperature up to 300°C) showed a gradual disappearance of martensite and formation of an ordered bcc lattice. The diffraction patterns over most of the sample area showed either a (111) or (110) diffraction in reciprocal space, although (100) and some higher order patterns were also observed at places.

The diffraction patterns taken at 100°C showed no trace of martensite and the corresponding structure confirmed this. The (110) and (100) patterns at this temperature, and above, showed strong superlattice spots as expected.

The interesting observations were, however, made on cooling the specimen from 300°C down to room temperature. After stabilizing the specimen for about 20 minutes at 300°C, it was allowed to cool slowly and electron diffraction patterns observed at intervals of 20°C after allowing sufficient time at each temperature for thermal stabilization. No change was observed in the patterns up to nearly 100°C (this temperature

varied somewhat with the composition and thermal history of the alloy). At 100°C however, faint diffuse spots were observed in the centre of each of the four "quadrants" in the (110) pattern (shown schematically in figure 10(a)). The spots initially appeared at places corresponding to "A". In most cases, however, the "A" spots were observed to split into two diffuse spots "A_1" and "A_2" in line with the super lattice spots corresponding to {001} and {111} reflections, on further cooling. No changes were observed up to this stage in the (111) diffraction pattern.

The (110) diffraction pattern at 60°C showed some more extra spots corresponding to "quadrupling" of "{200} repeat distance" - represented by "B" spots in figure 10(b). The (111) pattern also started to show some spots corresponding to a "tripling" of the "{110} repeat distance", at this temperature. A complete set of six "satellites" was observed (in the (111) pattern) around each Bragg reflection on further cooling.

A set of diffraction patterns over a range of temperatures are given in figures 11 and 12, showing the extra spots appearing in (110) and (111) patterns.

The same observations were reproduced on other fresh foils, except for a slight variation in the exact temperature of appearance (or disappearance, on heating) of these extra spots.

On reheating the foils, the spots were observed to disappear in the sequence C-B-A. A number of thermal cyclings of the foils gave the same results in sequence, as discussed above.

On further cooling, or aging the above foils at room temperature for some time, it was observed that at places, the "tripling" of the

"{110} repeat distance" had been replaced by highly diffused reflections that corresponded to an exact "doubling" of the same distance. This observation was in conformity with that made by Dautovich and Purdy (7) for the presence of the rhombohedral transition phase. The foil at this stage showed a mixture of patterns corresponding to "tripling" and "doubling" of the "{110} repeat distance" in the (111) pattern, and the (110) pattern with "A" and "B" spots.

In a few cases, usually involving diffraction patterns from areas close to the edge of the thin foils, diffused "streaks" were observed. These ran through the Bragg spots in a characteristic direction. An example of such diffraction patterns is shown in figure 13.

5.2 Nature of Thermal Diffuse Scattering

The sequential appearance of the extra spots on cooling, and their disappearance in reverse sequence on heating, suggests a reversible continuous structural modification that manifests itself in the form of these spots. As discussed in Section 3.9, structural disorders can be either linear, or planar. If the disorder is linear, i.e. the atoms move in a certain direction preferentially, it should appear as diffuse discs in the reciprocal lattice. No such diffuse discs are observed, and so, the possibility of linear disorder must be discarded.

Planar disorder, i.e. a certain family of planes vibrating in some characteristic direction, will result in diffuse streaks or "rel-rods" in reciprocal space. These diffuse streaks may result from phonons of certain amplitude and wave length, that are coupled together due to

the anharmonicity of the lattice. Assuming that large amplitude phonons are the cause of the diffused streaks, the extra spots or "satellites" may be postulated to be the intersections of the diffuse streaks on the Ewald sphere. The very symmetrical nature of these satellites indicates that these diffuse streaks run in a characteristic, identifiable direction in reciprocal space, with a certain unique temperature dependence of the length of the streaks. The spots or "satellites" are thus, intensity maxima at the points of intersection of these streaks, which do not themselves lie on the surface of the reflecting sphere.

The extra spots observed in the diffraction patterns are not due to formation of any superlattice in localized areas, as no complete correspondence is observed in the positions of these spots on (111) and (110) patterns. The electron diffraction patterns are all consistent with the initial postulate made, i.e. they are intensity maxima at the intersections of diffuse streaks that run in a characteristic direction.

(a) Direction of Streaking

A thorough analysis of the position, and sequence of appearance and disappearance of the extra spots in the diffraction patterns, leads to the conclusion that the streaks run in <210> direction in reciprocal space. The reciprocal lattice of a body centred cubic lattice is a face centred lattice. On streaking all the nodes in reciprocal lattice in <210> directions, it is observed that both (110) and (111) diffraction patterns with all the extra spots can be reproduced exactly.

(b) Temperature dependence of length of streaks

It is seen that the sequence of appearance or disappearance of extra spots in the diffraction pattern, with the postulate that these are the intersections of diffuse streaks running in <210> directions in reciprocal space, is in complete agreement with the hypothesis that the length of the streaks increases with decreasing temperature. Such a hypothesis would suggest an increase in the amplitude of thermal agitation of planes in <210> directions with decreasing temperature. This is consistent with the displacive nature of the parent-transition phase transformation.

Not much quantitative information regarding the temperature dependence of the length of streaks could be obtained from the present set of experiments, due to the absence of any tilting arrangements in the heating stage used. No patterns in the precise plane of the streaks were ever observed. Some observations, with a slight tilt from the Bragg condition, were made at room temperature with the thermally cycled foils, in the standard object stage which had tilting arrangements. They all confirmed the <210> directions of streaking.

(c) Confirmatory observations

(i) An exact quadrupling of "{200} repeat distance" in (110) diffraction, and a simultaneous tripling of "{110} repeat distance" in the (111) diffraction can only be obtained with the <210> direction of streaking.

(ii) A six-fold symmetry of satellites around each Bragg reflection on the (111) plane of diffraction can only be expected from streaks running in <hkl> direction in reciprocal space.

(iii) Since no streaks are observed in any (111) or (110) diffraction patterns when the specimen foil is exactly at Bragg condition, the direction of streaking has to be such that corresponding Bragg reflections do not appear in the (111) and (110) patterns. Any plane of diffraction containing {210} Bragg reflections should show streaks running through these reflections towards the origin. Neither (111) nor (110) diffraction patterns have any {210} Bragg reflections.

(iv) Some streaking is observed in (111) diffraction pattern at slight tilting of the specimen foil about one of the {110} axes. The "satellites" on Bragg spots lying on this tilt axis disappear while streaks, highly diffused, are observed through the rest of the Bragg spots in the pattern. This confirms the earlier postulate that the extra spots are intersections of streaks on the plane of diffraction. One set of such electron diffraction patterns is shown in figure 14.

(v) Figure 14 represents a sequence of diffraction patterns observed when a gradual tilt is given to the (111) plane of diffraction about a {110} axis, towards the (110) plane of diffraction. It shows streaks that run in a manner such that they intersect, on extrapolation, at a spot closer to the undeviated primary beam spot than the expected (200) Bragg reflection on the (110) (figure 14(c)) pattern. This can be explained clearly from the existence of <210> streaks.

Various other tilts performed on the specimen foil confirm these observations.

(vi) The postulate that the length of the streaks increases with decreasing temperature can be confirmed by considering the sequence of appearance of spots "A", "B" and "C".

The first spots to appear on cooling are the "A" spots. These are caused by the intersection of streaks from two (110) Bragg spots nearest to the (110) plane of reciprocal space. This is shown in figures 15(a) and (b).

Two spots "A_1" and "A_2", close together, are expected from the <210> streaks intersecting in the quadrant PQRS of the (110) plane of reciprocal lattice. Sometimes, only one diffused spot is observed at point "A". This may be expected in view of the closeness of the (110) plane to the nodes responsible for the corresponding streaks.

It can be shown that the minimum length of the streaks for the appearance of "A" spots has to be 0.234Å^{-1}, while "A_1" and "A_2" will appear at nearly 0.25Å^{-1} length. Similarly, it can be shown that the minimum length of the streaks for the appearance of "B" and "C" spots has to be 0.492Å^{-1}. This can be seen from figure 16 for "C" spots.

If the reciprocal space is defined by the equation:

$$a.a^* = b.b^* = c.c^* = 1$$

then, $|\vec{k}| . \lambda = 1$, where λ is the wavelength of the phonon and $\vec{k}$ is the "propagation vector".

The shorter the wave length, the longer the streaks in reciprocal space. Thus, at the Brillouin zone boundary, where the streaks are caused by some components of a standing wave, a minimum wave length exists that gives streaks long enough to intersect at the extra spots in the diffraction patterns.

5.3 Instability in the Lattice of the Parent Phase

The <210> direction of streaking implies that in real space, the {210} planes distort more easily in <210>directions, or have a very strong component of any resultant mode of distortion in these directions. Guinier (17) has stated that in a layered structure like graphite, the directions of strong streaking are those in which the crystal is most easily distorted. Thus, in generalization of this observation, it can be inferred that the vibrations of {210} planes normal to themselves are more intense than those parallel to these planes, whatever the direction of propagation of waves in these planes. The regular periodicity of the crystal is thus modulated such that the diffuse scattering is concentrated in <210> directions as streaks, in reciprocal space.

It is obvious from the discussion in Sections 3.5 and 3.6 that only the acoustic modes of vibration are involved and the effect of optical modes is neglected. Another reason for doing so is that the optical modes depend primarily on the difference in the atomic masses. In TiNi the constituent atoms Ti and Ni do not differ much in their masses, so that the TiNi crystal behaves more or less like a monoatomic crystal. Optical modes are not very prominant in monoatomic (or similar)crystals.

The fact that the length of the streaks increases with decreasing temperature indicates that the wavelength of the corresponding large amplitude thermal waves decreases with decreasing temperature.

The thermal energy in a particular mode of vibration consists of two parts - kinetic and potential. A decrease in the elastic constants

results in an increased amplitude of vibration in the particular direction and a corresponding increase in velocity. In order to conserve the thermal energy, the frequency must go down (to balance the effect of increased amplitude) with decreasing temperature. The number of phonons increase at the same time. A drop in frequency as shown in figure 17 is predicted (qualitatively) near the First Brillouin zone boundary, with decreasing temperature. This indicates an incipient instability in the system as the temperature is lowered and the frequency tends to zero (28). The limit is defined by zero frequency of vibration in which the system "freezes" and a phase with a new kind of unit cell is expected. A similar instability is seen in systems which show stacking faults (30), where the length of the diffuse streaks is seen to increase as the probability of faulting increases.

5.4 Mode of "Freezing"

Buerger (11) has analyzed this type of instability in terms of atomic displacements. As the degree or amplitude of thermal agitation increases, a stage is eventually reached when the atoms swing past their natural point of equilibrium (or "nodes") and overcome the non-nearest neighbour attractions. The new structure is determined by the atomic movements in some resultant direction.

The most plausible mode of distortion based on the postulates mentioned in Sections 5.2 and 5.3, is explained in figure 18. The atomic movements in the (010) plane of the lattice are as shown in figure 18(a). Atoms A_2 and B_1 move towards each other while atoms A_1 and B_2 move apart

along <101> directions. All the actual contacts between atoms that may be said to touch are maintained, and only the non-contacting atoms are displaced with respect to one another. Thus, no disruption of any linkage of the nearest neighbours in the lattice occurs. The net result is a cooperative displacement of atoms as shown in figure 18(b) in a three dimensional lattice. The exact amounts or magnitudes of such displacements can be determined by a critical analysis of the distortion, involving the force constants between atoms in appropriate directions, variation of elastic constants with temperature, and the "packing" problem involved.

This mode of distortion of the parent phase lattice can be obtained by resolving the net displacements into two components. These components can be shown to be associated with two transverse acoustic (shear) waves in the lattice with wave lengths $2d_{001}$ and $2d_{110}$. The "propagation vectors" ($\vec{k}$) of these waves lie normal to (001) and (110) planes, and the polarization vectors lie in <100> and <001> directions respectively, as shown by dark filled arrows in figure 18(b). It is to be noted that in the direction of the cube axis <001> the two transverse modes tend to mix with one another and the polarization vector in the transverse plane is not unique. In such cases, the polarization vector is usually fixed by symmetry arguments (since the wave vector $\vec{k}$ coincides with a symmetry axis of the crystal).

The resultant phonons have wave vector in <111> directions and a wave length of $2d_{111}$. The net effect of such a perturbation is a prominant (strong) vibration of {210} planes in anti-correlation with a strong component normal to themselves, which causes strong diffuse streaks in

<210> directions of reciprocal space. The vibration of <210> planes can be seen to have a wave length of $2d_{210}$ (even though it does not exist physically in the lattice). The individual components of vibration of all other planes in directions normal to themselves, in anti-correlation, can be seen to be either very weak ({221} planes, for example) or negligible, so that strong diffuse streaks are limited to <210> directions only in reciprocal space.

The net distortion of the lattice can thus be associated with a standing wave at the First Brillouin zone boundary (with a wave length $2d_{111}$) for an ordered CsCl structure, with component phonons having wave lengths $2d_{001}$ and $2d_{110}$ respectively.

In the above analysis, qualitative as it is, no reference has been made to the other kind of atoms present in the lattice that occupy the body centred positions in a simple cubic lattice of the other. The two kinds of atoms are, however, expected to behave in the same manner as described above and the lattices of each kind are postulated to distort in the manner described above. The body centred atoms are postulated to remain undisplaced while the lattice of the other atoms is being distorted. At the Brillouin zone boundary, where a standing wave exists, this postulate does not seem unreasonable. The net distortion, and the mode of "freezing" will depend on the easiest mode of "packing" the two kinds of atoms together in the transformed structure.

From the lattice vibration dispersion curves (frequency vs $\vec{k}$ vector), discussed in Section 3.11, and the above analysis, it is

expected that one of the acoustic modes of vibration will approach zero frequency at the onset of instability. A behaviour such as the one shown in figure 17 is postulated for all three phonons with wave vectors at the centres of [001], [110] and [111] zone faces. A unique identification of such a mode will, however, require a determination of complete dispersion curves, taking into account the changes in elastic constants with temperature. Such an analysis is not possible at the present stage due to non-availability of a good sized single crystal (see Appendix B) of TiNi. However, it can be hypothesized that the instability will set in first with respect to the transverse acoustic mode of vibration with the coupled wave vectors at the centres of [001] and [110] zone faces.

An analysis of the kind discussed above applies only at or close to the transition temperature. The lattice parameters "b" in figure 18(b) have changed in each individual unit cell along the Y-axis, but the effect is averaged out if similar modes of distortion at any instant of time are considered in (100) and (001) planes in adjacent domains in the lattice. The distortions discussed above do not result in a rhombohedral structure when the lattice "freezes" according to the model in figure 18(b). However, a tendency for some net distortion in the <111> directions on "freezing" is predicted from the above analysis. It can be postulated that at the transition temperature, the atoms are able to overcome the nearest neighbour attraction forces and a number of symmetry elements appear and disappear abruptly so as to give a resultant distortion of the unit cell in <111> directions. Such a distortion will eventually result in a rhombohedral structure with a lattice parameter

exactly double that of the parent phase.

Wang, et al (6) observe a tripling of the unit cell at the transition temperature. Their zero layer Buerger (precession) x-ray patterns show streaks in some <210> directions that split into spots that correspond to a tripling of the unit cell. They have attributed this to a substitutional order-disorder of the parent lattice. The extra spots that appear in place of the <210> streaks can be treated as eight satellites around each {210} Bragg reflection, and this configuration is obtained when a "freezing" of the lattice with a number of phonons having wavelength $3d_{210}$, is presumed at the first Brillouin zone boundary of a "disordered" bcc structure. This is not in agreement with the observations of the present investigation.

5.5 The Transition Phase (Dark field Microscopy)

The formation of the rhombohedral transition phase is somewhat analogous to an order-disorder transformation with the "superlattice" of rhombohedral cell having a lattice parameter $a_o = 6.02\mathring{A}$. The neighbouring ordered regions or domains may have different orientation in space and it is thus possible to reveal them in transmission electron microscopy by the diffraction contrast produced by the domain boundaries.

Diffraction contrast may be produced in a two phase structure by several possible things (31).

If the neighbouring domains have different "sublattice", so that an anti-phase boundary is formed at the interface, the structure is revealed by the diffraction contrast from the APBs. These APBs may be of climb type or shear type.

In addition to the APBs, domain structure may be formed by semi-coherent boundaries between adjacent local areas of crystallographic distortion. The adjacent areas may have related orientations if the distortion is due to a co-operative phenomenon. Contrast is produced in such cases partly from the imperfection structure of the boundaries, which are elastically distorted with respect to the matrix or surrounding areas. The contrast in such a micrograph is not determined by the structure within these locally distorted domains alone, but depends also on the structure and imperfections in the matrix. This contrast is similar to the "orientation contrast" seen in cases of coherent superlattice.

Other types of contrast from a second phase are: (a) displacement fringe contrast - when the second phase displaces the matrix planes in opposite directions on either side of it. (b) Moire fringe contrast - from the Moire fringes formed by two superimposed crystal lattices of different lattice spacing and/or orientation, (c) interface contrast - due to the curvature of the interface, and the bending of the lattice planes near the interface. The last named is often associated with other types mentioned above.

Experimentally, in dark field images, diffraction contrast is produced by placing the objective aperture in the system which lets through a diffracted beam. The contributions to the image come from a narrow column in the direction of the diffracted beam, about 20Å in diameter, for a thickness of crystal nearly 1000Å. The intensity of the image varies as ∿

$\frac{\sin^2 \pi ts}{(\pi s)^2}$, where t is the crystal thickness and s is the

deviation parameter as shown in figure 19.

It can be shown that maximum contrast is to be expected when $\frac{1}{\lambda} \sim s$ λ being the wave length of displacement of atoms along the diffracting column (depth oscillations).

In the "displaced aperture technique" of dark field microscopy, the image suffers from poor contrast due to the effects of spherical aberration of the objective lens and astigmatism. This elongates all image points along the direction joining the centre spot of diffraction pattern to the selected diffraction spot. This elongation becomes more serious for higher order reflections.

The effect of spherical aberration on resolution can be removed by centering the chosen diffracted beam along the optical axis of the microscope by tilting the gun. Images of very high resolution can be obtained from this technique. A loss in illumination intensity is unavoidable in this technique, especially for higher order reflections, unless a realignment of the illuminating system is done on each diffracted beam chosen. The gain in resolution, however, more than outweighs this small inconvenience.

The gain in resolution is obtained primarily by a change in phase shift across the undeviated and diffracted beam obtained by tilting. Chromatic aberration effects are removed completely as the phase shift is equal and opposite in direction for the two beams. The minimum resolvable spacing d, which is given by $d = \lambda/\alpha$ for the displaced aperture method, is improved to $d = \lambda/2\alpha$ due to equal and opposite phase spread from spherical aberration, α being the beam divergence as shown in figure 20.

In the case of a domain structure, as observed in the "superlattice" of rhombohedral phase, diffraction contrast is observed (due to domain boundaries) only when certain superlattice reflections are used. No contrast is obtained from any other reflection. High contrast dark field images of the rhombohedral phase can be obtained by using any of the first order "superlattice" spots (which appear as doubling spots of "{110} repeat distance" in a (111) diffraction pattern) and projecting its image. No fringe contrast is observed from the domain boundaries in bright field, as they lie parallel to the plane of the film. Periodicity in such domains as in the present case, shows up very well in some of the dark field photographs (figures 21 to 25).

The photographs suggest a moderate degree of co-operation between adjacent domains. This, however, is expected from the displacive nature of transformation.

In such cases of orientation contrast, a certain degree of interface contrast is always involved due to the accompanying curvature and bending of the interface planes caused by distortion of the lattice.

CHAPTER VI

CONCLUSION

The present investigation confirms that under favourable conditions, the martensite formation in TiNi is preceded by the formation of a transition phase by a diffusionless, second order transformation. The transition phase forms as a result of a postulated mechanical instability in the parent CsCl structure on cooling. This incipient instability shows itself in the form of localized thermal diffuse scattering, which has been found in this investigation to arise from a planar disorder in the parent lattice. Extra spots or "satellites" that appear over a temperature range prior to the formation of the transition phase, are shown to be the intersections of diffuse streaks on the Ewald sphere.

These diffuse streaks run in <210> directions in reciprocal space indicating prominant vibration of {210} planes in anti-correlation in these directions. The component phonons are associated with two transverse acoustic modes which are always coupled and have wave lengths $2d_{001}$ and $2d_{110}$ respectively. The resultant phonon has a wave length $2d_{111}$.

The streaks intersect at the zone boundary where a λmin exists that gives streaks long enough to generate all the extra spots in the diffraction patterns.

A two dimensional model for displacement of atoms in a resultant <101> direction is suggested for each (010) plane of the lattice, and it generates the same structure in three dimensions when two transverse

MILLS MEMORIAL LIBRARY
McMASTER UNIVERSITY

acoustic modes of perturbation with wave lengths $2d_{001}$ and $2d_{110}$ are postulated.

Instability sets in in the system when one of the acoustic modes of vibration tends to zero frequency, when the system "freezes".

The suggested model for distortion of the unit cells of parent phase does not yield a rhombohedral cell on "freezing". It is postulated that the analysis applies only at the transition temperature, where the atoms overcome the nearest neighbour attraction forces and result in a net distortion along <111> directions. This eventually leads to rhombohedral symmetry.

Dark field micrographs of the transition phase show that it forms in a domain structure, with a moderate degree of co-operation between adjacent domains.

CHAPTER VII

SUGGESTIONS FOR FUTURE WORK

1. The failure of some workers to observe any phase transformation in TiNi over a range of temperature -20°C to 600°C has been attributed to a too high oxygen content in their alloys. Though much has been said and done on the importance of oxygen, more work is needed to clarify its role.

2. A better, quantitative understanding of the temperature dependence of length of the streaks is required to explain the incipient instability in the parent lattice on cooling. A double-tilting heating stage is necessary for these observations.

3. The proposed mode of distortion is based on the postulate that the structure is being distorted by two transverse acoustic modes (phonons) having wave lengths $2d_{001}$ and $2d_{110}$. Lattice dynamics should be applied to calculate the net amount of such distortions taking into account the variation of elastic constants with temperature.

4. The instability in the parent phase lattice is postulated to set in when one of the acoustic modes of vibration tends to approach zero frequency. Complete neutron dispersion curves should be determined to identify this mode uniquely. A fair sized single crystal of the alloy is necessary for such a study.

APPENDIX A

Volumetric Measurements

Volume changes associated with the formation of triclinic martensite phase were determined using a vacuum sealed Mercury dilatometer (figure 26). The specimen for this set of experiments was prepared from the as-cast 50% Ni alloy ingot obtained from the argon arc melting furnace by hot swaging the ingot down to roughly a rod form with diameter approximately 1/2". A length of approximately 1 1/4" was taken and a cylindrical specimen of volume 2270 cu. mm (density = 6.55 gm/cm^3) was prepared by turning the rod on a lathe machine.

The cylindrical specimen was electro-polished, then sealed in a vycor tube under 10^{-6} mm Hg vacuum for annealing. Annealing was done at 500°C for 24 hrs. The surface of the specimen showed no discolouration.

The specimen so obtained was immersed completely in liquid nitrogen for over an hour to ensure a completely martensitic structure.

The specimen was then placed in the dilatometer bulb and the whole unit evacuated, with the open end of the lower capillary (horizontal) in a mercury filled beaker and the stop cock closed. After a vacuum of the order 10^{-5} mm Hg. was recorded in the bulb, the top end of the dilatometer (vertical capillary) was closed and the stop cock opened. The mercury rushing in from the beaker displaced any air still present in the unit, which was evacuated again by repeating this procedure several times until no air bubble remained in the unit. The

level of mercury in the capillary (vertical) was allowed to set at a convenient arbitrary value on a scale.

The bulb of the dilatometer was then immersed completely in a Haake Unitherm temperature controlled oil bath, and the level of mercury in capillary noted at fixed temperature intervals, with a caliberated telescope and vernier scale. Similar procedure was used for both the heating and cooling cycles. The specimen was thermally cycled between room temperature and 150°C.

A sudden increase in volume of the specimen was observed on cooling at nearly 65°C, and an equivalent volume decrease on heating at about 95°C, as shown in figure 27. The exact temperatures of reversion of martensite to parent phase on heating, and the formation of martensite on cooling, were confirmed as 95°C and 65°C by resistivity (resistance vs. temperature) measurements on the same sample.

The change in volume (on heating or cooling) was found to be 1.232 cu. mm., or approximately 0.054%. This is almost one tenth of the volume change reported by Wasilewski (32).

Similar runs were made on 51% Ni alloy and an exact reproduction of data was obtained (except for different temperatures of reversion) in this case. The changes were found to be completely reversible and repeated cycling gave a reproduction of the curve in figure 27.

The measurement of volume changes thus acts as an additional check in the determination of reversion temperatures of the martensitic transformation product, which have up to now been determined primarily by resistivity methods. The volume changes measured by a vacuum sealed

mercury dilatometer are closest to the theoretically expected changes from the cell constants (lattice parameters) of the parent phase and the triclinic martensite as reported by Dautovich and Purdy (7).

APPENDIX B

Preparation of Single Crystals of TiNi

Several attempts were made, using various techniques, to grow single crystals of the alloy.

At first, methods involving the liquid state were tried under a high vacuum in an electron beam zone-melting unit. The sample rod (prepared from a combination of hot and cold rolling of the ingot button and swaging of a roughly square section so obtained into cylindrical rod form) was mounted at both ends in holder clips, with a circular tungsten filament, encircling a narrow zone of the rod, acting as heat source. The filament was fixed to a carriage driven by an overhead motor with controllable speed. The heating of the sample rod, by radial emission of electrons when the current was passed through the filament, was concentrated in a thin narrow zone about 1 mm in height, by the use of two molybdenum shields on either side of the filament. The shields were fixed to the carriage assembly. A fairly accurate control of temperature and speed of the carriage was possible. Temperature was controlled by a control of the emission current, voltage.

The chamber holding this assembly was evacuated to better than 10^{-6} mm Hg vacuum before each run. A sudden drop in vacuum was observed each time the heating was started, but it improved with time in each case.

A zone of molten liquid (about 1 mm in height) was made to travel several times, every time in the same direction in a certain

fixed length of the sample rod, to enable some crystal with a favourable orientation to grow preferentially at the expense of other smaller crystals. After innumerable attempts, all resulting in near failure, this technique was given up. After a few runs, the sample rods invariably started showing second phase precipitate which would hinder growth of any crystal.

"Strain-anneal" techniques (solid state) were then used on sample rods of varying sections,composition, thermal history, etc. A critical stress was determined on an annealed sample by the standard tensile test-metallography method. It was found to be 23.05 D^2 tsi, D being the diameter of the specimen in inches. The apparatus to hold the specimen rod was modified, in that the top end of the rod was left free and the bottom end fixed to a water cooled copper block, to provide a thermal gradient along the length of the rod. The hot zone - the specimen being within 50 - 60° of the melting point - was passed along the strained sample rod at very slow speed (about 1 - 2 mm/hr.), moving away from the cold end. Care was taken to control the temperature and speed of travel of the hot zone so that no incipient melting was ever observed. A few such runs on a 51% Ni alloy sample resulted in large grains on the surface of the rod, with at least one of them showing a tendency to grow preferentially. At such a stage, the hot zone was allowed to pass several times on the particular region of the specimen without straining it, to enable that crystal to grow. After a few runs, no further growth was noticed.

The sample was then cut up to examine the section at this crystal front.

Unfortunately, a bi-crystal (two single crystals, each of approximately 2 - 3 mm. in diameter, 6 mm. in length) was obtained in section. The orientation of the single crystals so obtained was determined by Laue back reflection of x-rays, and the zone axis was found to be close to [221], which was of not much use.

APPENDIX C

X-Ray Intensity Measurements

Intensity measurements of Bragg reflections were made on the diffractometer traces of TiNi to check for the CsCl structure of the alloy, and were found to be in fair agreement with the theoretically expected values. The diffractometer traces (obtained by using Cu k_α radiation with LiF monochromator and Ni + Co balanced filters) of Starke and Lee (10) were used for these calculations, and the results are given in Table II. The calculations confirm the existence of CsCl structure in TiNi.

Calculations were also made of the intensity of diffuse scattering from the "background" in x-ray powder patterns of the transition phase. A brief discussion, to follow, will show how the r.m.s. displacements of atoms in certain crystallographic directions were calculated from the intensity of thermal diffuse scattering.

The background in a x-ray powder pattern consists of (i) a general, incoherently scattered, radiation consisting of Compton scattering, Debye - Jauncey scattering, etc., and (ii) a coherently scattered thermal diffuse radiation.

The intensity of this thermal diffuse scattering (TDS) depends on, among other things, Bragg angle, atomic displacements, atomic scattering factor of elements involved, etc. Photo-densitometer

runs were made across three such x-ray powder patterns, taken at 50°, 45° and 23°C for an earlier investigation of transition phase by Dautovich and Purdy (7). Approximate values of TDS were calculated from these traces, after correcting for Compton scattering, from the background. No anisotropy of atomic vibrations about their nodes was assumed.

The intensity of TDS is proportional to the mean square displacement $\langle \overline{U}_x^2 \rangle$ of the atoms in any direction x, temperature factor, etc. Corrections for Compton scattering were applied using the assumption:

$$I_{background} = I_{Compton} + I_{TDS} \qquad (1)$$

$I_{Compton}$ was taken as:

$$I_C = \{Z - \sum_{j=1}^{Z} \left| f_{jj}^2 \right| \} \left(\frac{\nu^1}{\nu}\right)^3 \qquad (2)$$

where ν and ν^1 are frequencies of x-rays before and after scattering, and $(\sum \left| f_{jj}^2 \right|)$ is the sum of all "Incoherent Scattering factors", taken from standard tables.

I_{TDS}, obtained from equations (1) and (2), was taken as:

$$I_{TDS} = \sum (f_{kk})^2 \cdot (1 - e^{-2M}) \qquad (3)$$

where f_{kk} is the scattering factor, and M is given by:

$$M = 8\pi^2 \langle \overline{U}_x^2 \rangle \left(\frac{\sin \theta}{\lambda}\right) \qquad (4)$$

M, for simplicity, was assumed to have the same value for Ti and Ni atoms under the isotropic assumption.

The average value of $\langle \overline{U}_x^2 \rangle$ or mean square displacement was calculated from above equations for important crystallographic directions and is given in Table III. It can be clearly seen from these approximate calculations that contrary to the normal case, the atomic vibrations increase with decreasing temperature.

The general increase in the thermal diffuse scattering with decreasing temperature indicates that the crystal is becoming more isotropic, which spreads the diffuse scattering uniformly over the powder pattern.

TABLE 1

Composition of Alloys and
Heat Treatment Schedule

Alloy No.	Composition (in atomic %)	Annealing Temperature T_A	Time at T_A
A-1*	51% Ni	700°C	1 hour
A-2	50.5% Ni	650°C	24 hours
A-3	50.5% Ni	650°C	96 hours
A-4	51% Ni	650°C	24 hours
A-5	51% Ni	650°C	96 hours
A-6	51% Ni	(i) 700°C	20 hours
		(ii) 500°C	96 hours
A-7**	50% Ni	500°C	96 hours

* See section 4.2

** Used for volumetric and single crystal work only.

TABLE 2

Calculations of Intensity of Bragg Reflections

in X-Ray Powder Patterns of TiNi

Line Indices	$\frac{\sin\theta}{\lambda}$	Multiplicity factors	L.P. factors*	$\lvert F\rvert^2$	$\frac{I_{Theo.} \times 10^3}{I_o}$	$I_{obs.}$** (units)
100	0.166	6	22.4	27.6	3.71	0.375
110	0.235	12	17.18	1164.0	240.0	41.1
200	0.332	6	4.98	816.0	24.4	4.2
211	0.406	24	2.925	540.0	36.6	6.56

* Corrected for LiF monochromator in the diffractometer set up.

** Observed intensities are based on integrated intensity measurements from area under the Bragg peaks in diffractometer traces.

TABLE 3

Calculation of $\langle \bar{U}^2 \rangle$ from I_{TDS}

Line Indices	$\frac{\sin\theta}{\lambda}$ ($\mathring{A}^{-1}$)	I_c (e.u)	I_{TDS} (e.u.) 50°C	45°C	23°C	e^{-2M} 50°	45°	23°	$\langle \bar{U}^2 \rangle \times 10^{-3}$ 50°	45°	23°
110	0.235	6.86	0.69	8.23	15.09	0.999	0.987	0.977	0.138	1.443	2.635
200*	0.332	10.67	-	-	-	1.000	1.000	1.000	-	-	-
211	0.407	12.48	2.61	9.47	16.70	0.993	0.974	0.955	0.275	0.995	1.772
220	0.470	14.40	10.30	20.27	23.62	0.966	0.932	0.921	1.008	1.998	2.348
310	0.522	∿ 18.24	18.21	32.24	48.02	0.930	0.876	0.815	1.678	3.058	4.725
222	0.575	∿ 18.24	31.16	43.50	83.29	0.850	0.790	0.598	3.465	4.515	9.830

* Since a minima existed in densitometer traces of all three patterns at this Bragg angle, the total background was taken as equal to Compton scattering at this value of $\sin\theta/\lambda$.

Dashed lines indicate zero values, taken as standard for calculations.

LIST OF REFERENCES

1. Duwez and Taylor, Trans. AIME, 188, 1173, 1950.
2. Pietrokowsky and Youngkin, J. Appl. Phys., 31, 1763, 1960.
3. Purdy and Parr, Trans. AIME, 221, 636, 1961.
4. Buehler and Wiley, Trans. ASM Qrtly., 55, 269, 1962.
5. Buehler, Gilfrich and Wiley, J. Appl. Phys., 34, 1475, 1963.
6. Buehler, Wang and Pickart, J. Appl. Phys., 36, 3232, 1965.
7. Dautovich and Purdy, Can. Met. Qrtly., 4, 129, 1965.
8. Wasilewski, Trans. AIME, 233, 1691, 1965.
9. Dautovich, Melkvi, Purdy and Stager, J. Appl. Phys., 37, 2513, 1966.
10. Starke and Lee, (to be published) Paper presented at International Conference on "Characterization of Materials", at Penn. State Univ., Univ. Park, Pa., November 1966.
11. Buerger, "Phase Transformations in Solids", J. Wiley, 1951, Ch. 6, p. 188.
12. Barrett, "Structure of Metals", McGraw Hill, 1962, Ch. 22, p. 579.
13. Ehrenfest, see Reference 15.
14. Landau and Lifshitz, "Statistical Physics", Clarendon Press, Oxford, 1938, Ch. 11, p. 204.
15. Tisza, "Phase Transformations in Solids", J. Wiley, 1951, Ch. 1, p. 1.
16. Born and Huang, "Dynamical Theory of Crystal Lattices", Oxford, 1954.
17. Guinier, "X-Ray Diffraction", Freeman, 1963, Ch. 6 and 7.
18. Wooster and Ramchandran, Acta Cryst. 4, 335, 431, 1951.
19. Ziman, "Electrons and Phonons", Clarendon Press, Oxford, 1960, Ch. 3, p. 133.
20. Cahn, Acta Met. 9, 795, 1961.
21. Woods, Cochran and Brockhouse, Phys. Rev., 119, 980, 1960.

22. Lyddane and Herzfeld, Phys. Rev., 54, 846, 1938.

23. Hanlon and Lawson, Phys. Rev., 113, 472, 1959.

24. Dick and Overhauser, Phys. Rev., 112, 90, 1958.

25. Cochran, Phy. Rev. Letters, 3, 412, 1959.

26. Hardy and Karo, Phil. Mag. 7, 315, 1962; and Phys. Rev. 129, 2024, 1963.

27. Szigeti, Trans. Faraday Soc. 45, 155, 1949.

28. Hardy and Karo, "Lattice Dynamics", Ed. Wallis., Pergamon, 1965, Ch. A27, p. 195.

29. Dick, Phys. Rev., 129, 1583, 1963.

30. Wooster, "Advanced Methods of Crystallography" Ed. Ramchandran, Acad. Press, 1964, Ch. 5, p. 121.

31. Hirsch, Howie et al, "Electron Microscopy of Thin Crystals", Butterworths, 1965, Ch. 7, 13, 14.

32. Wasilewski, Unpublished Report.

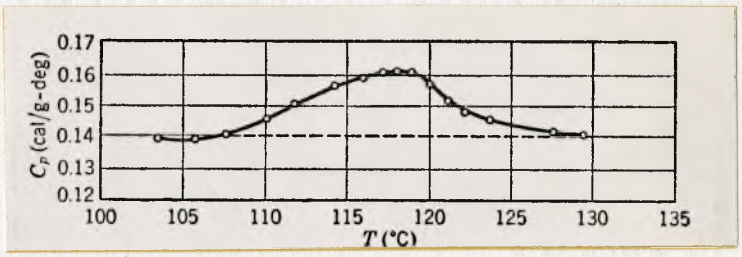

Figure 1

Specific heat of Barium Titanate (after Tisza, 15)

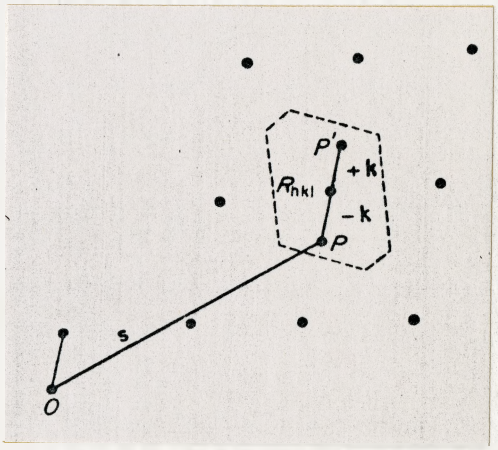

Figure 2

Satellites of the lattice point R_{hkl} corresponding to the wave whose propagation vector is k . The first Brillouin zone surrounding R_{hkl} is shown with a dashed line (after Guinier, 17).

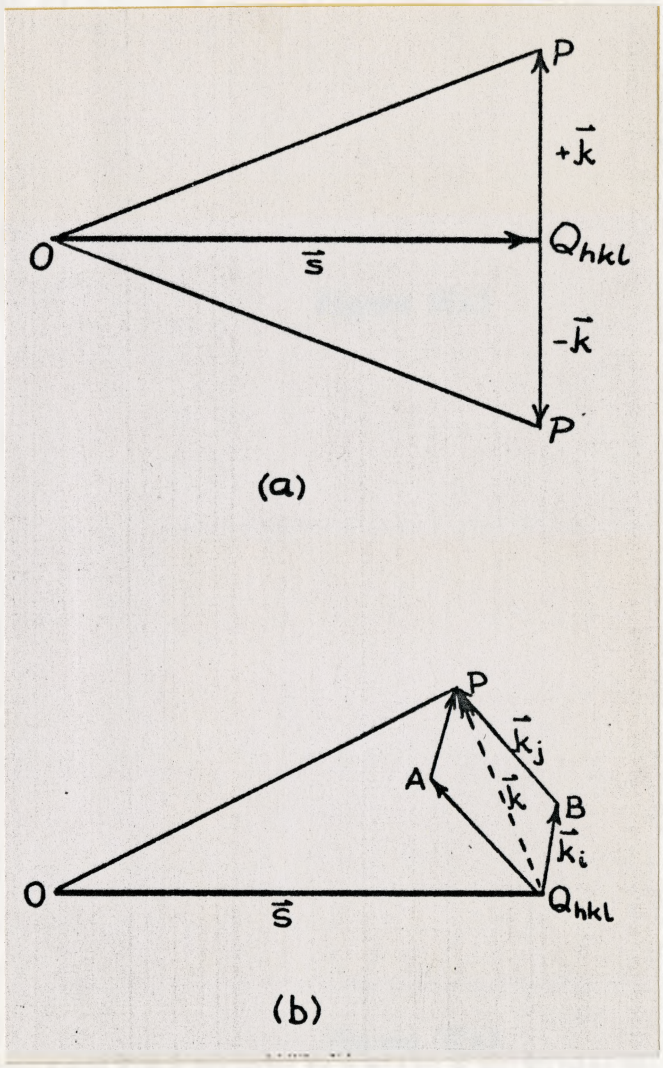

Figure 3

First and Second Order Scattering.

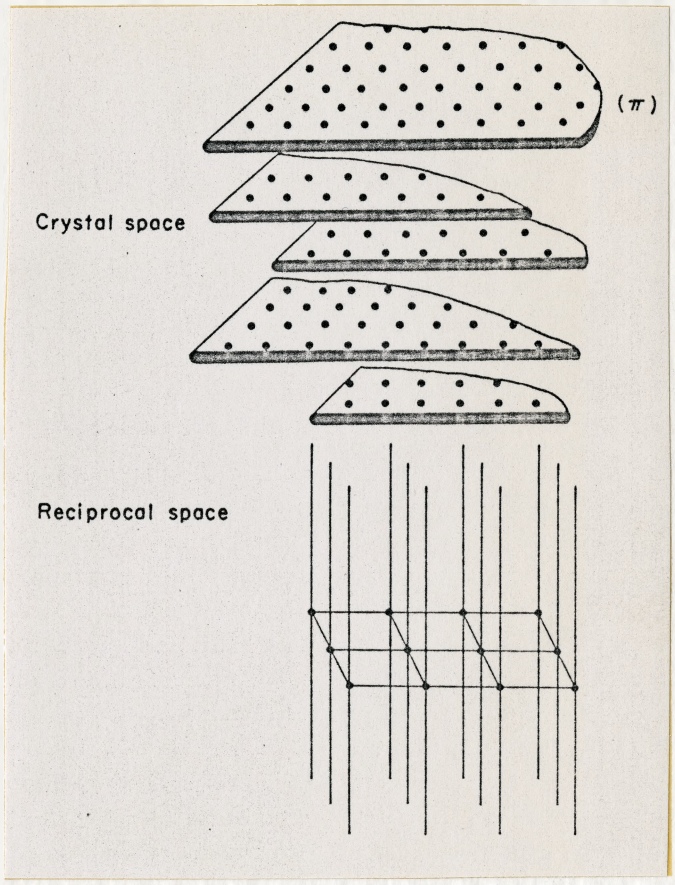

Figure 4(a)

Planar disorder (after Guinier, 17).

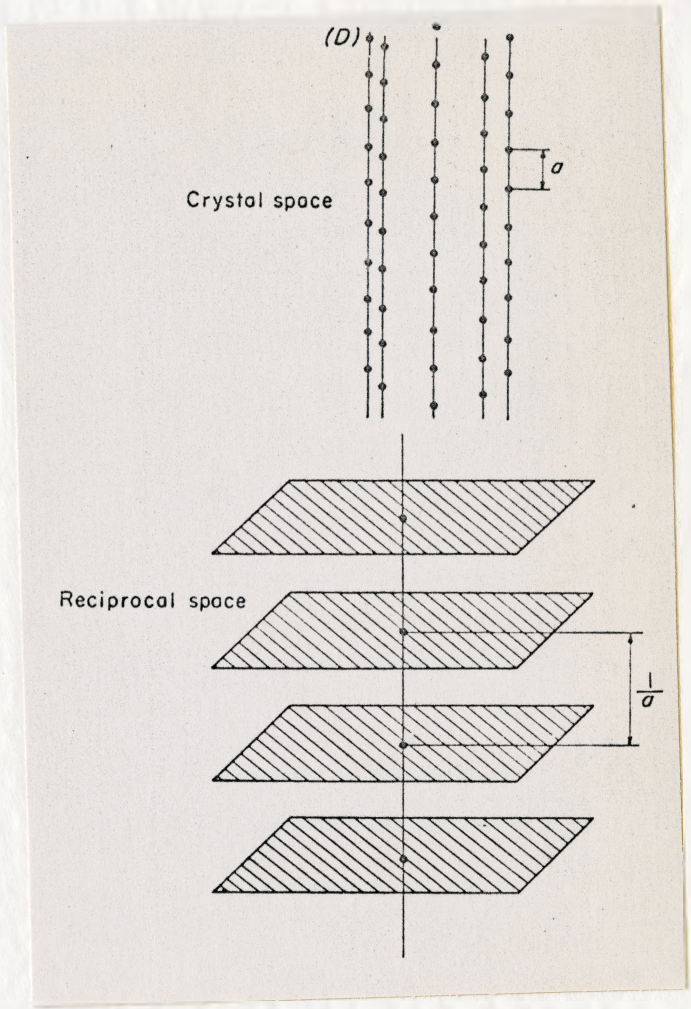

Figure 4(b)

Linear disorder (after Guinier, 17)

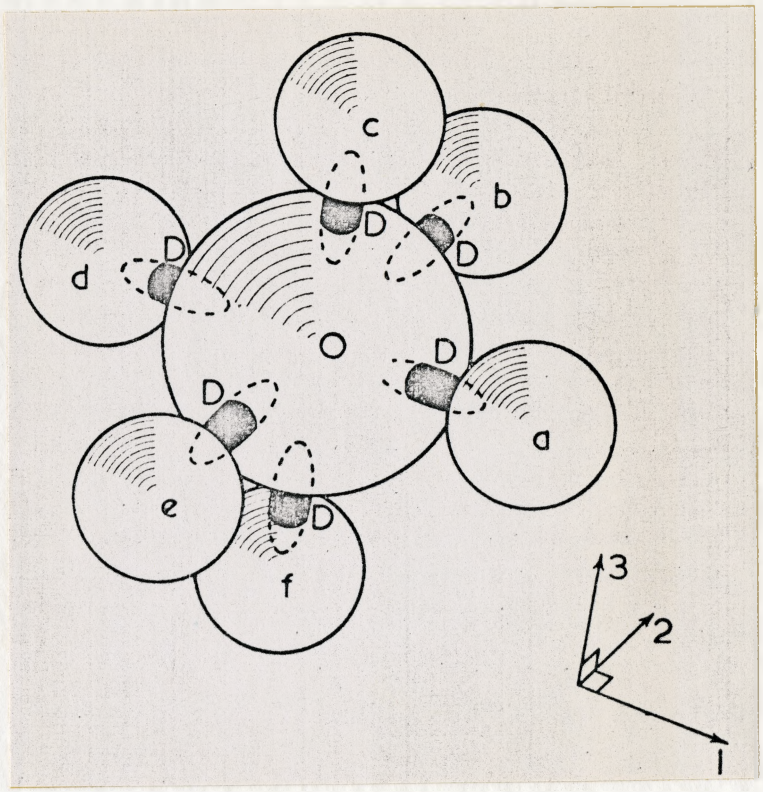

Figure 5

Model for the configuration of a Negative ion and its nearest neighbours in a NaCl structure. D represents the regions of maximum displaced charge density (after Hardy, 26(i).

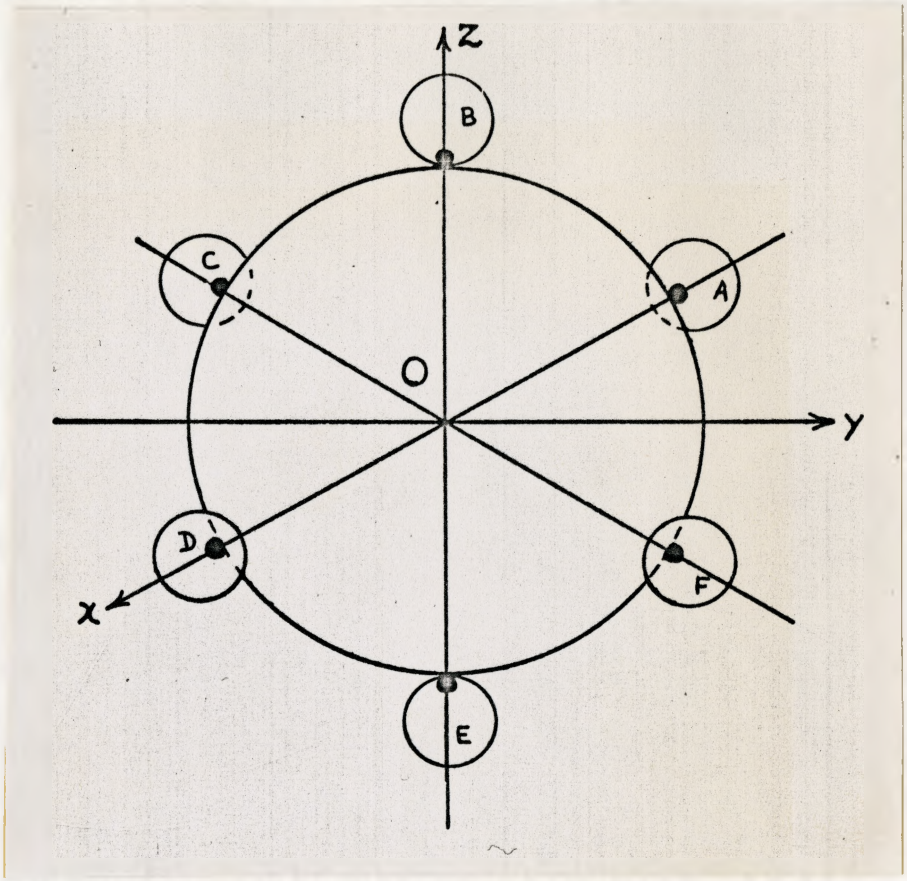

Figure 6

Schematic model for positions of exchange charges about a central negative ion in an unstrained lattice. Large and small spheres are negative and positive ions, filled small black circles are exchange charges (after Dick, 29)

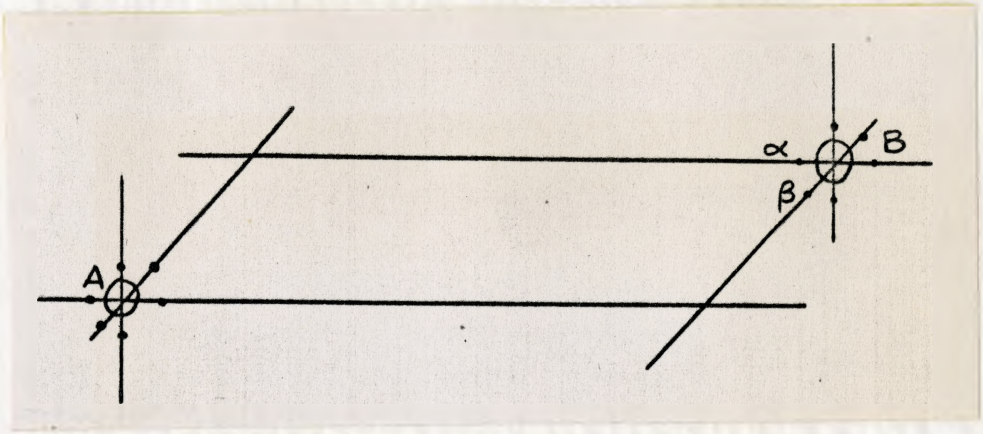

Figure 7

A pair of second nearest neighbour positive ions with their associated exchange charges indicates by small filled circles. The charge on B is modified due to the interaction of α and β with A (after Dick, 29).

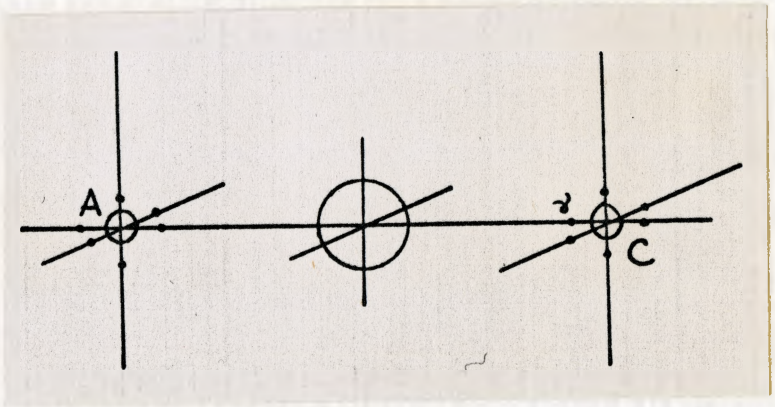

Figure 8

A pair of fourth nearest neighbours with associated exchange charges indicated by small filled circles. The charge on C is modified due to interaction of γ with A. (after Dick, 29).

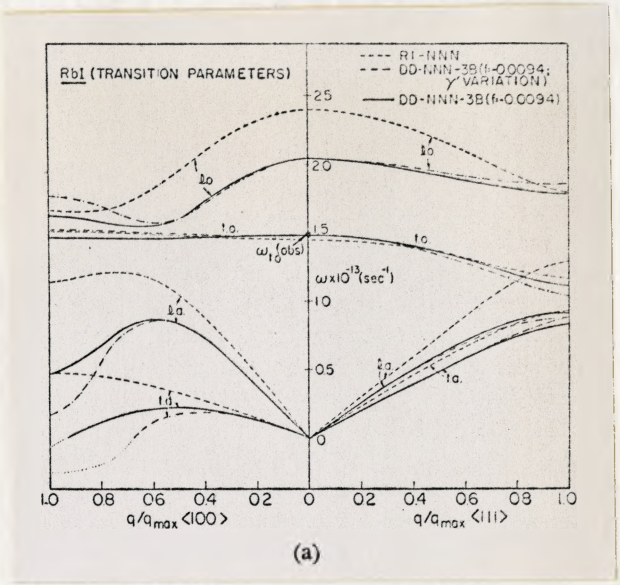

(a)

Figure 9(a)

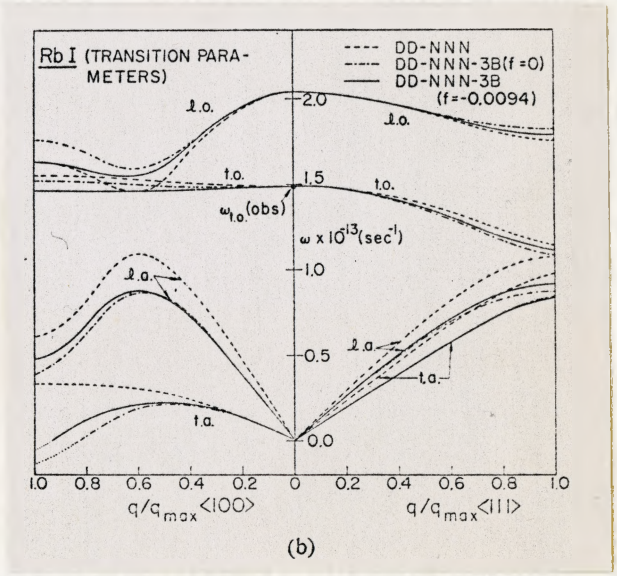

(b)

Figure 9(b)

Dispersion curves for the NaCl phase of RbI at the transition pressure (after Hardy and Karo, 28)

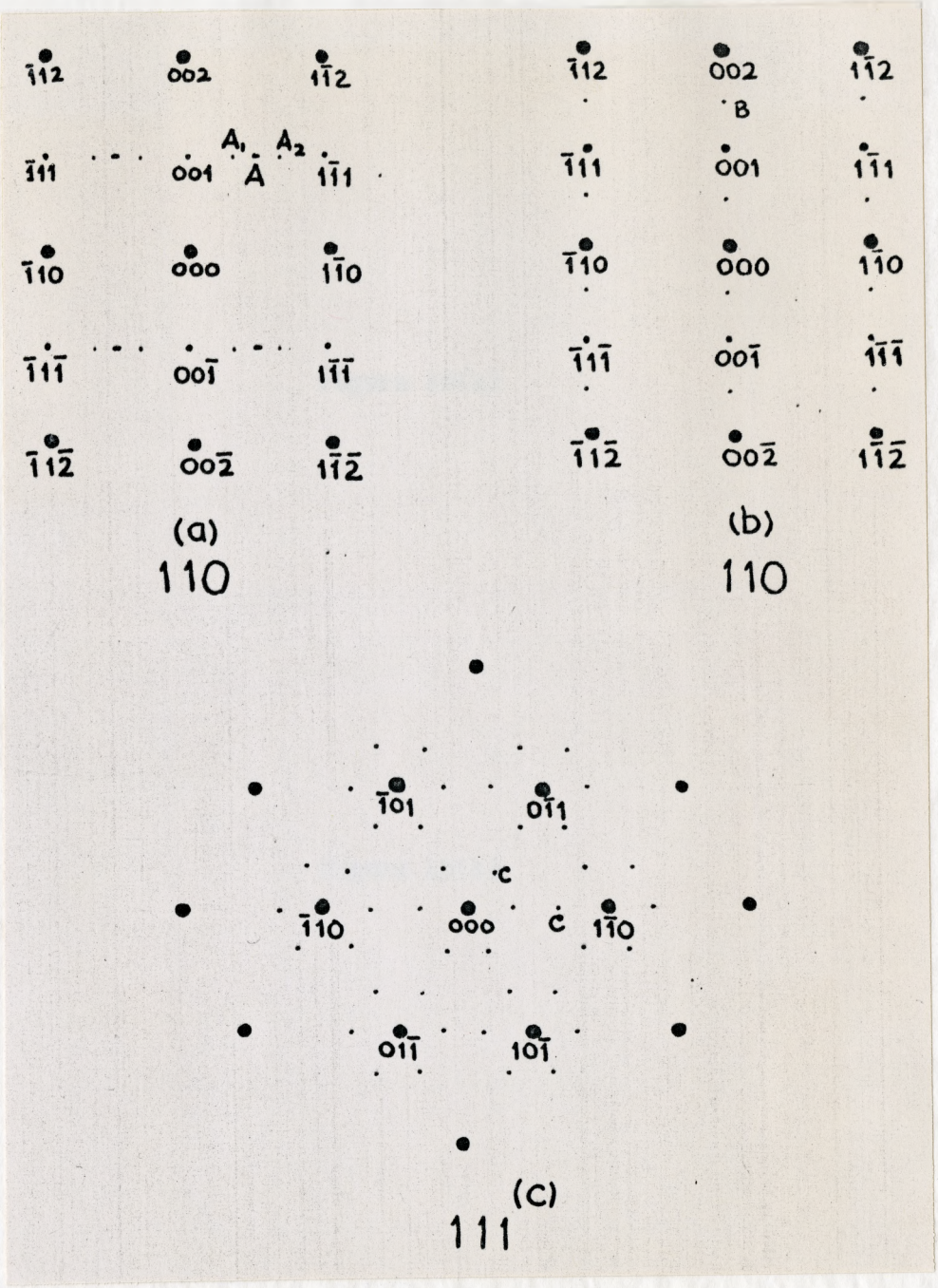

Figure 10

Schematic representation of "satellites" and extra spots in the electron diffraction patterns observed in thermal cycling of TiNi thin films. (a) spots "A", "A_1" and "A_2" in the "quadrants" of (110) pattern, (b) spots "B" in (110) pattern, (c) satellites "C" in (111) pattern.

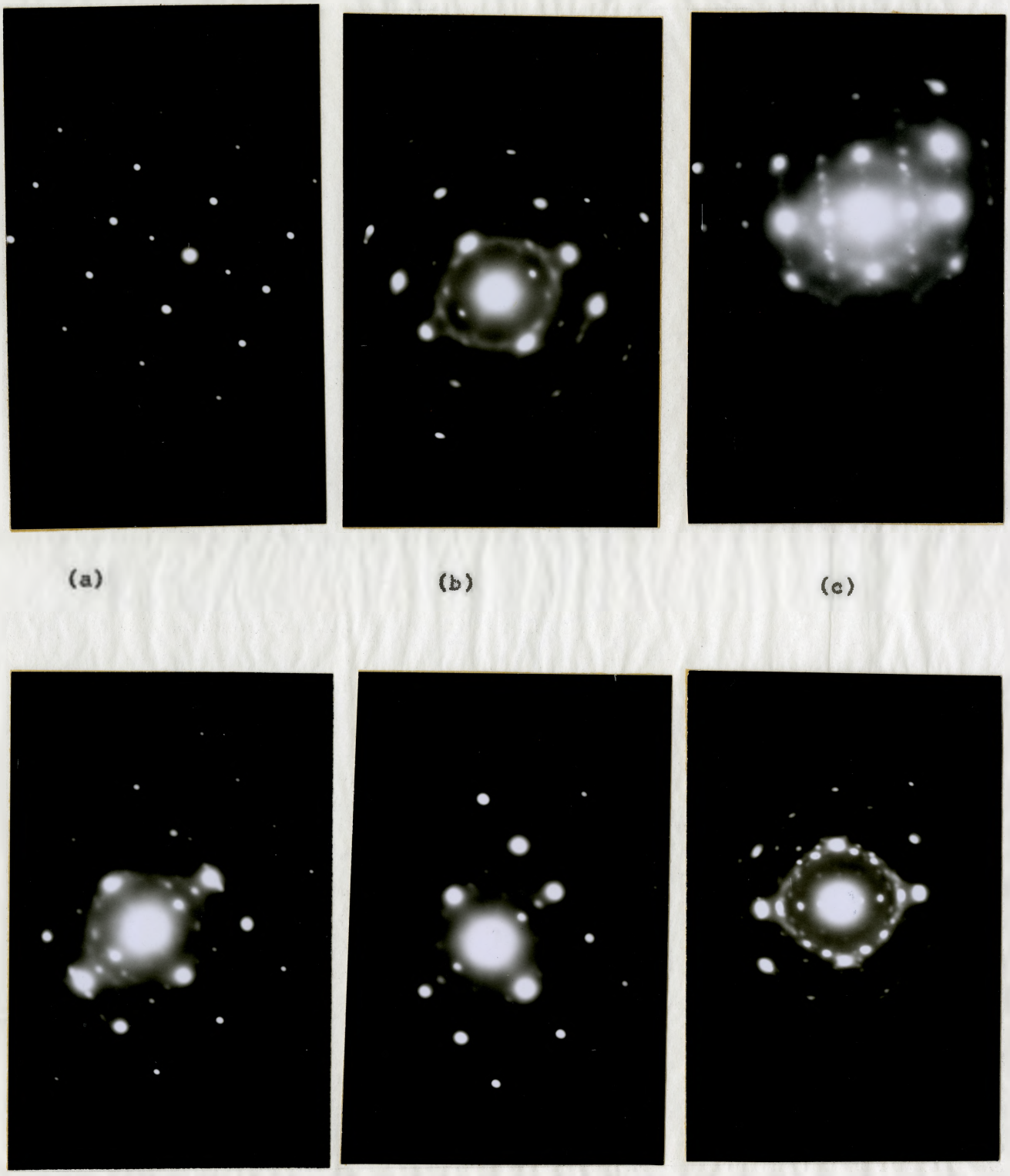

Figure 11 (a) to (f)

A series of (110) electron diffraction patterns from TiNi thin films observed at (a) 120°C, (b) 100°C, (c) 80°C, (d) 60°C, (e) near room temperature, (f) room temperature (with a slight tilt).

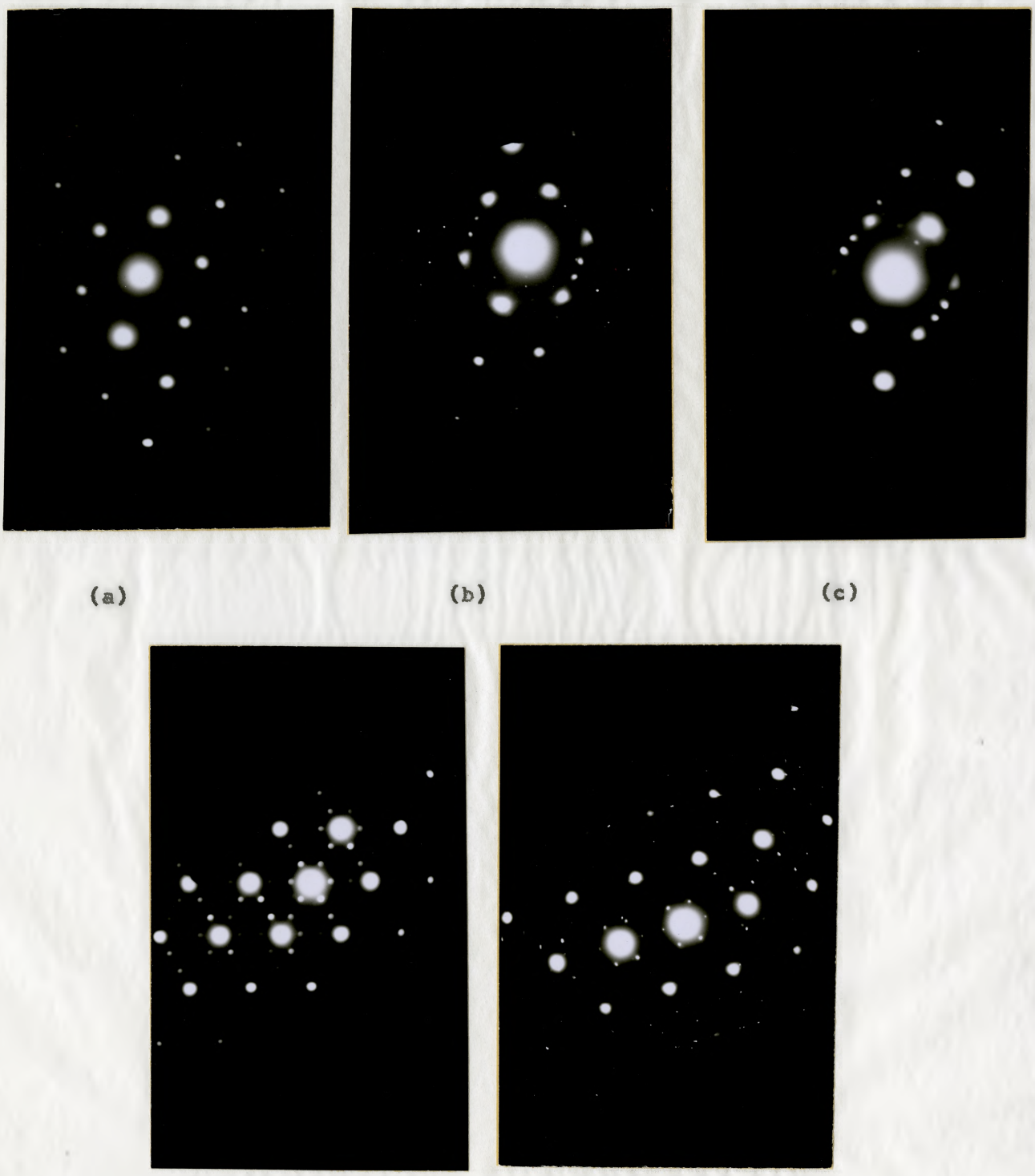

Figure 12

A series of (111) electron diffraction patterns from TiNi thin films observed at (a) 100°C, (b) 60°C, (c) 40°C, (d) near room temperature (e) on further cooling.

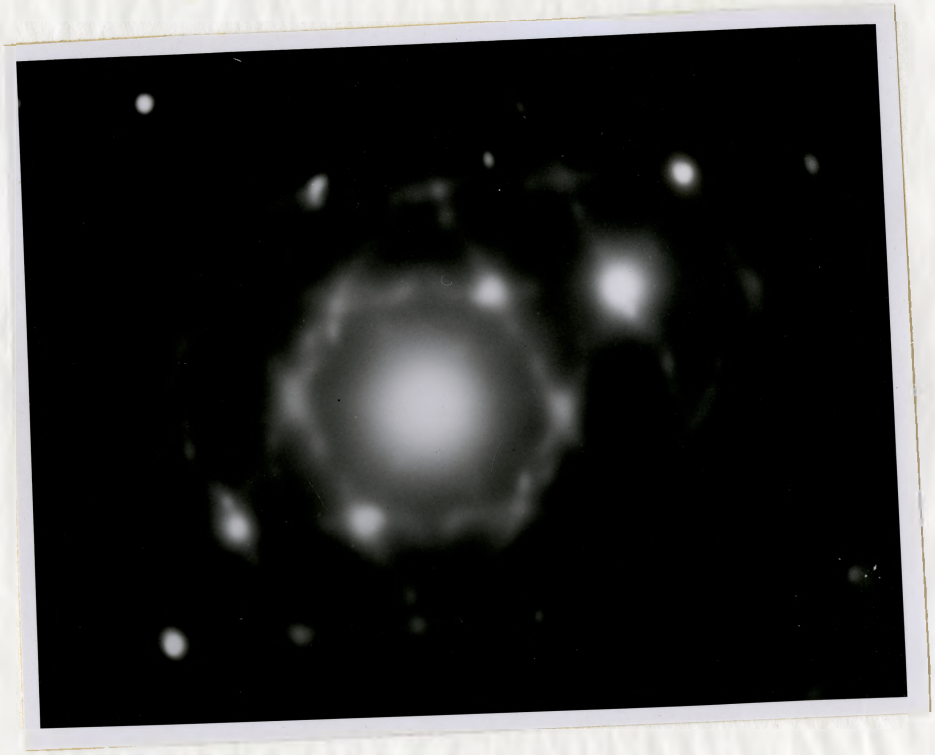

Figure 13

An example of streaks in (111) electron diffraction pattern, observed near the edge of a thin film.

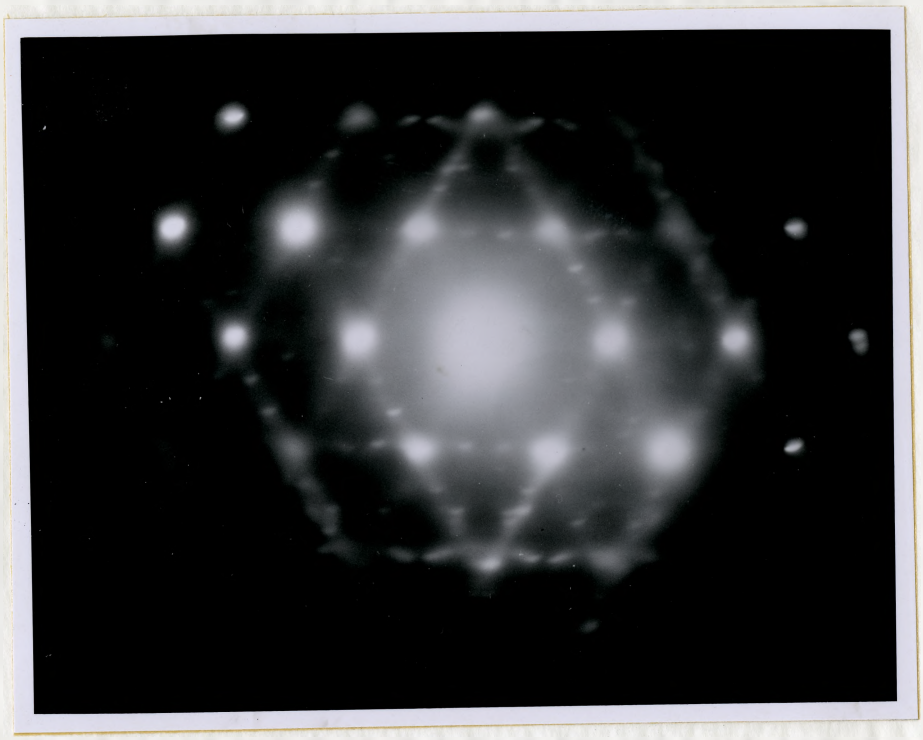

(a)

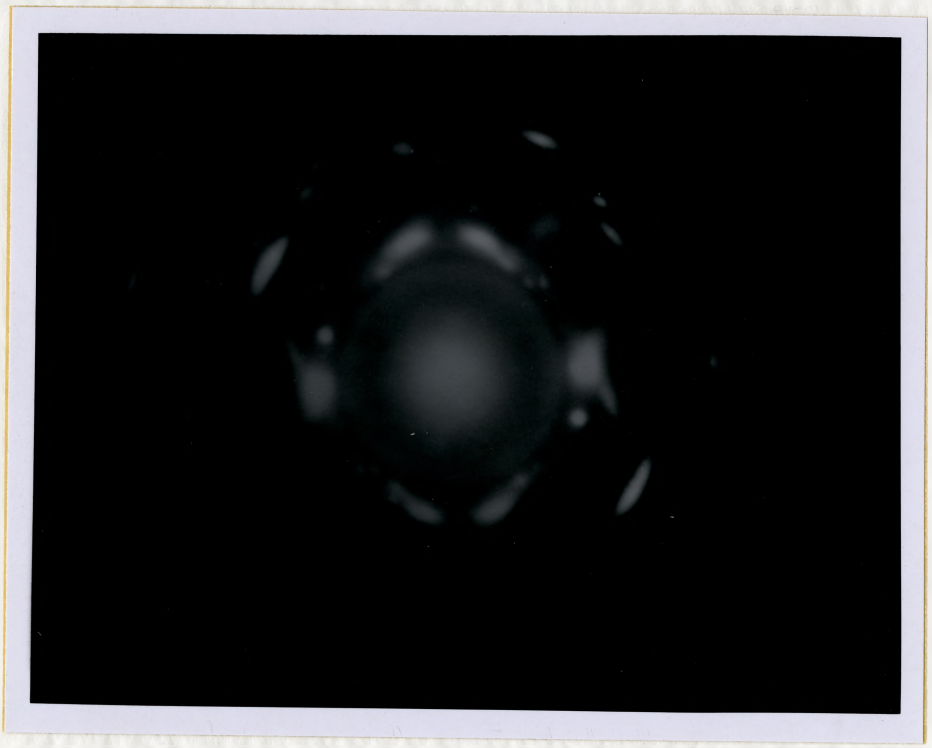

(b)

Figure 14
(continued)

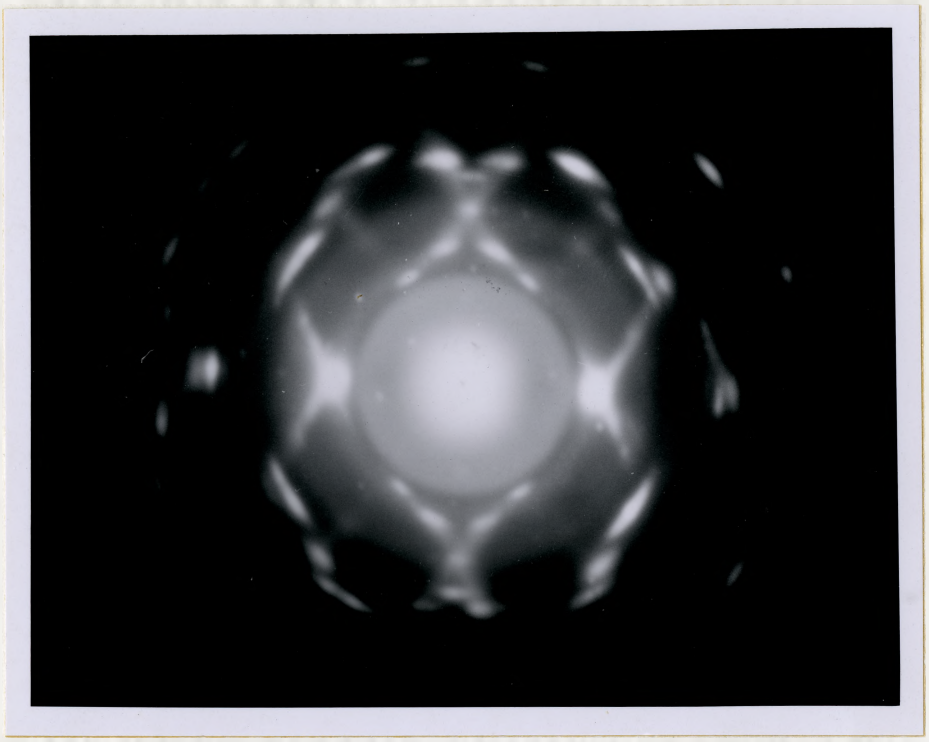

(c)

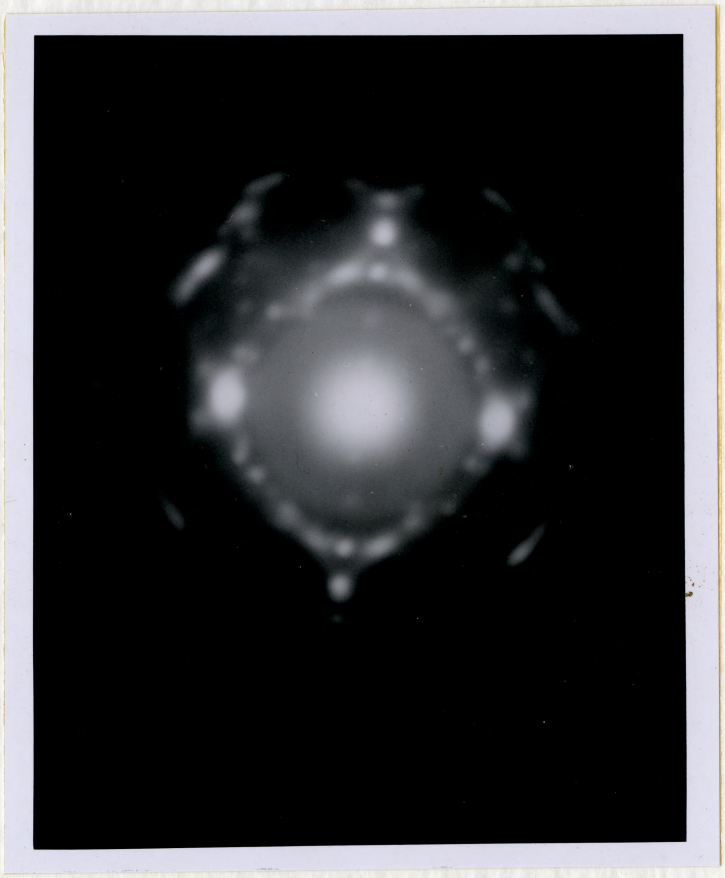

(d)

Figure 14 (Continued)

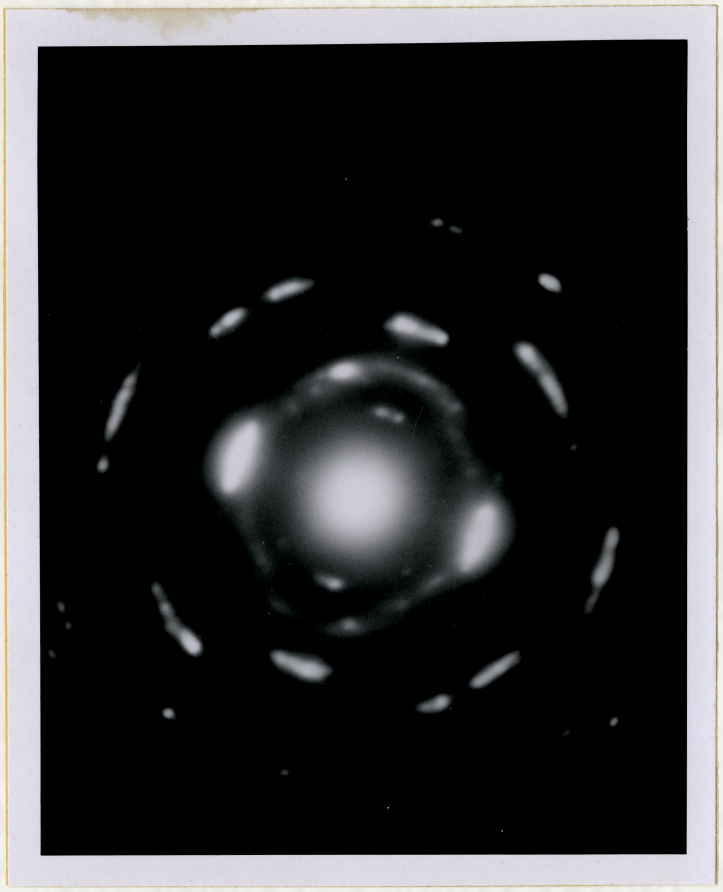

Figure 14(e)

Figures 14 (a to e)

A sequence of electron diffraction patterns showing streaks in (111) pattern observed on gradual tilting of the plane of diffraction about a {110} axis towards a (110) plane of diffraction.

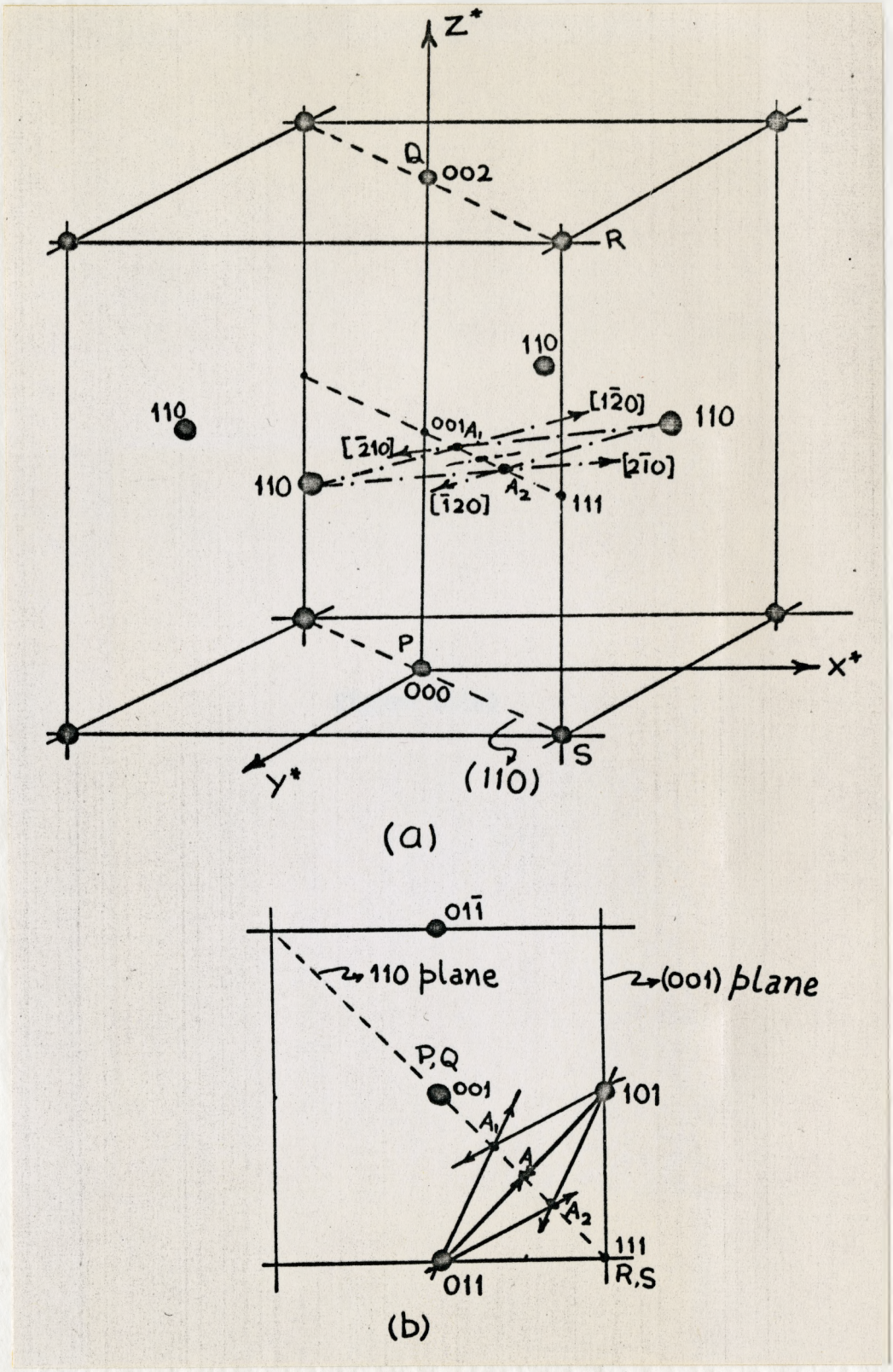

Figure 15

Temperature dependence of the length of streaks. Appearance of "A" spots (schematic).

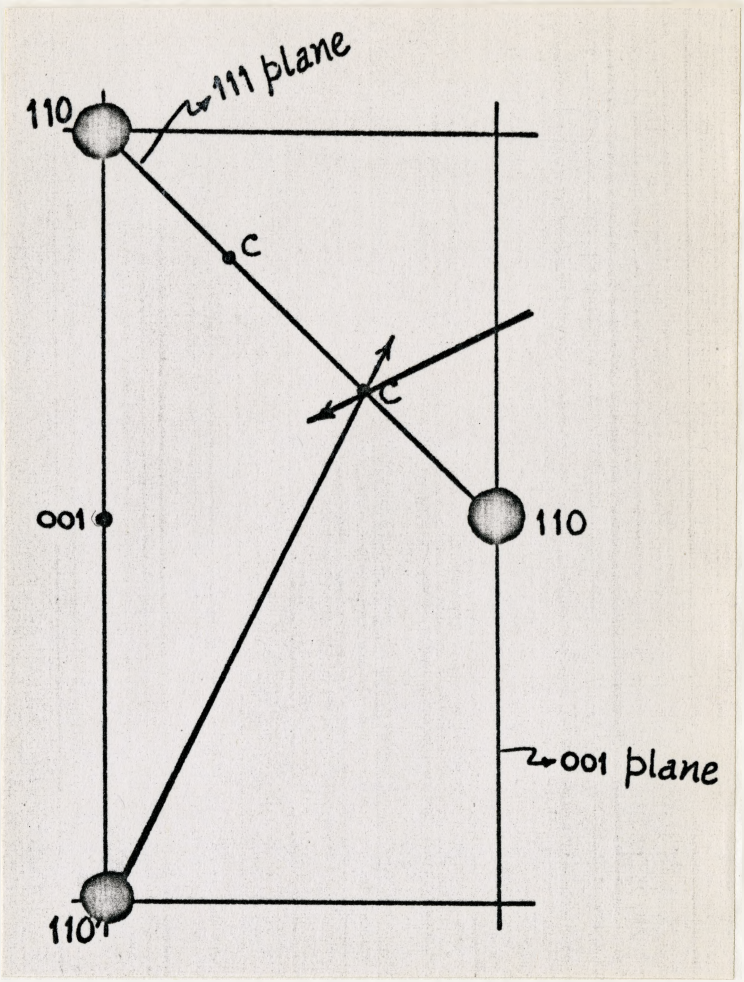

Figure 16

Temperature dependence of the length of streaks. Appearance of "C" spots (schematic).

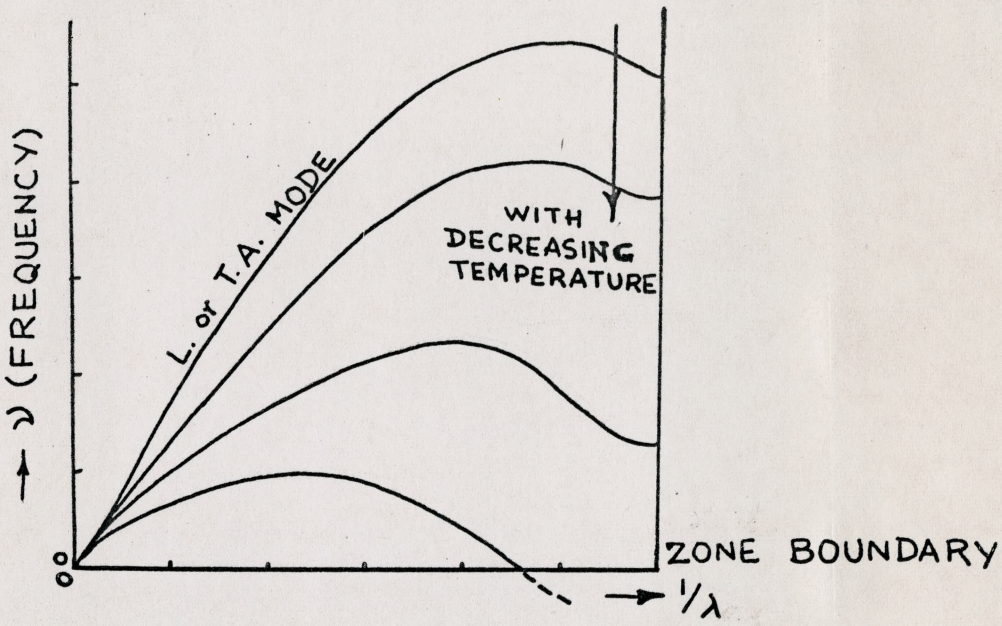

Figure 17

Suggested behaviour of the "acoustic" dispersion curves with decreasing temperature, for the parent CsCl lattice of TiNi.

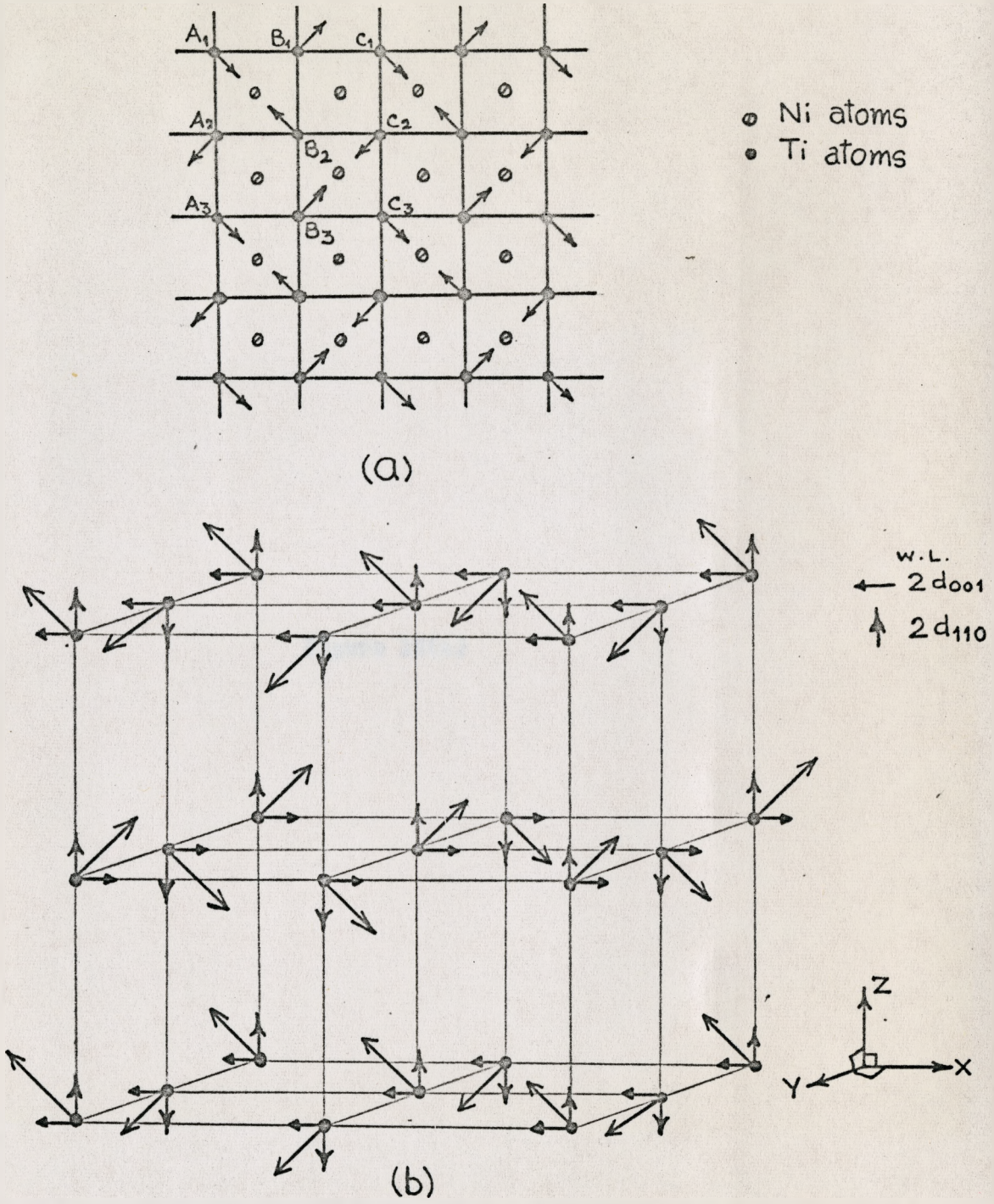

Figure 18

Suggested mode of distortion of parent phase lattice (a) in a (010) plane (b) in three dimensions, with resolved components shown by filled arrows. The components are associated with two transverse acoustic modes (or "phonons") of vibration, having wave lengths $2d_{001}$ and $2d_{110}$ respectively.

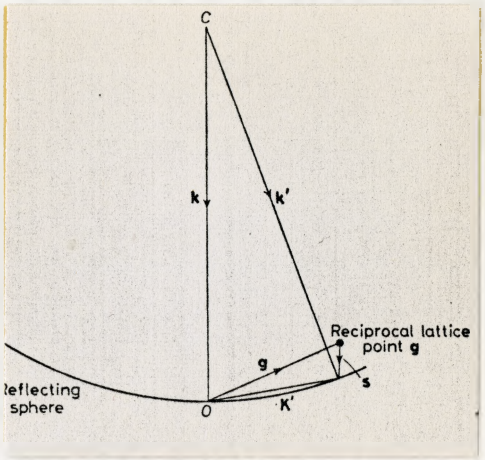

Figure 19

Definition of deviation parameter "S" (after Hirsch, et al.,31)

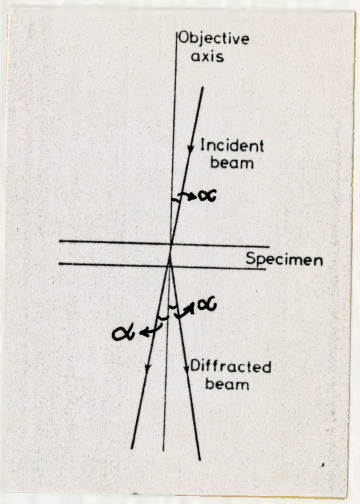

Figure 20

Definition of beam divergence "α" (after Hirsch, et al.,31)

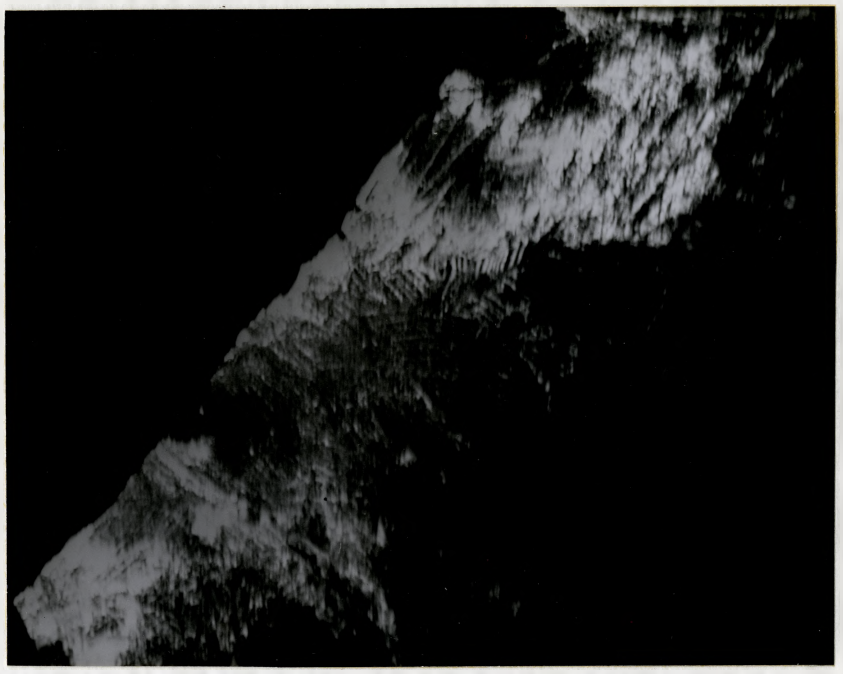

Figure 21

Dark field micrograph of the transition phase,x 20,000

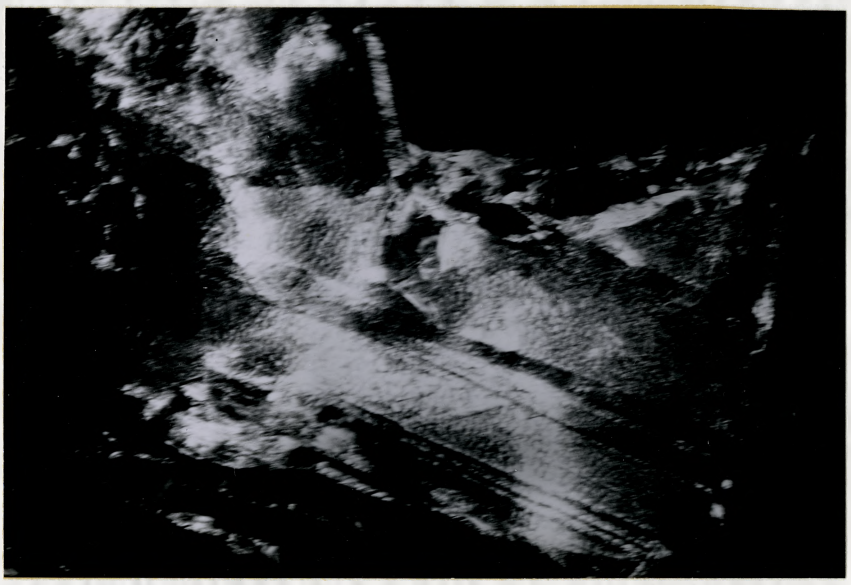

Figure 22

Dark field micrograph of the transition phase,x 20,000

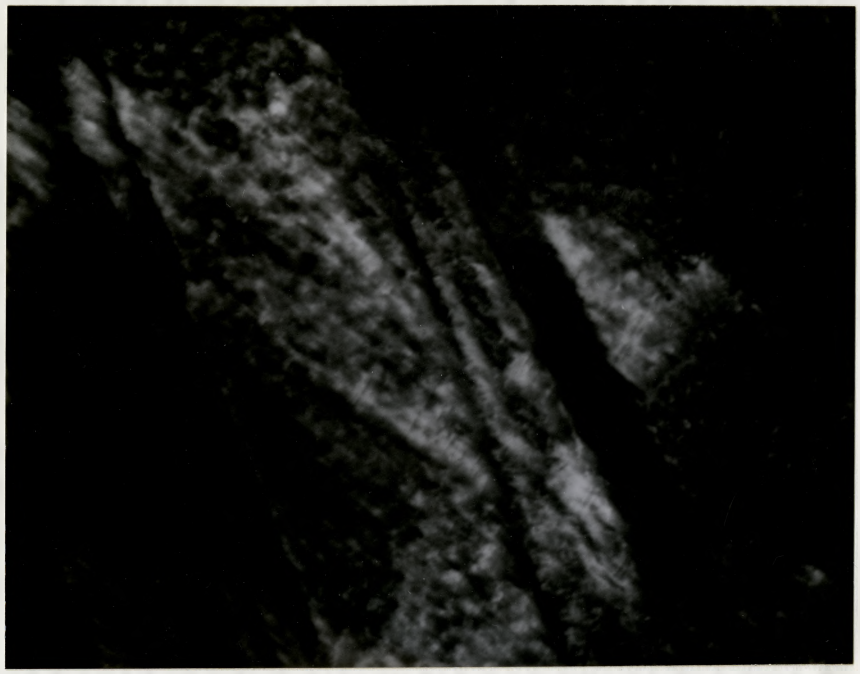

Figure 23

Dark field micrograph of the transition phase, x 60,000 (same in area as figure 22).

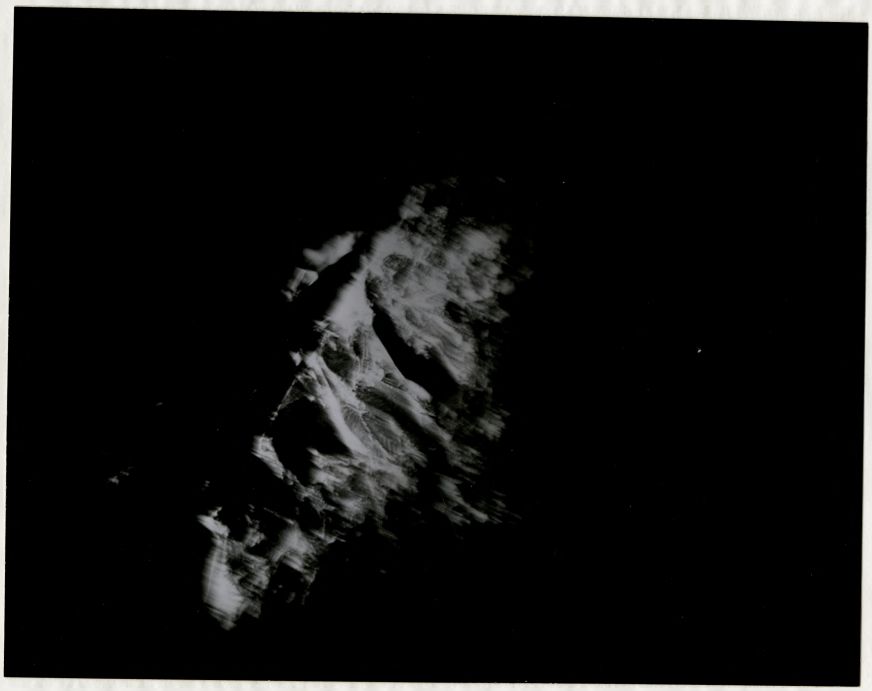

Figure 24

Dark field micrograph of the transition phase, x 20,000

Figure 25

Dark field micrograph of the transition phase, x 40,000

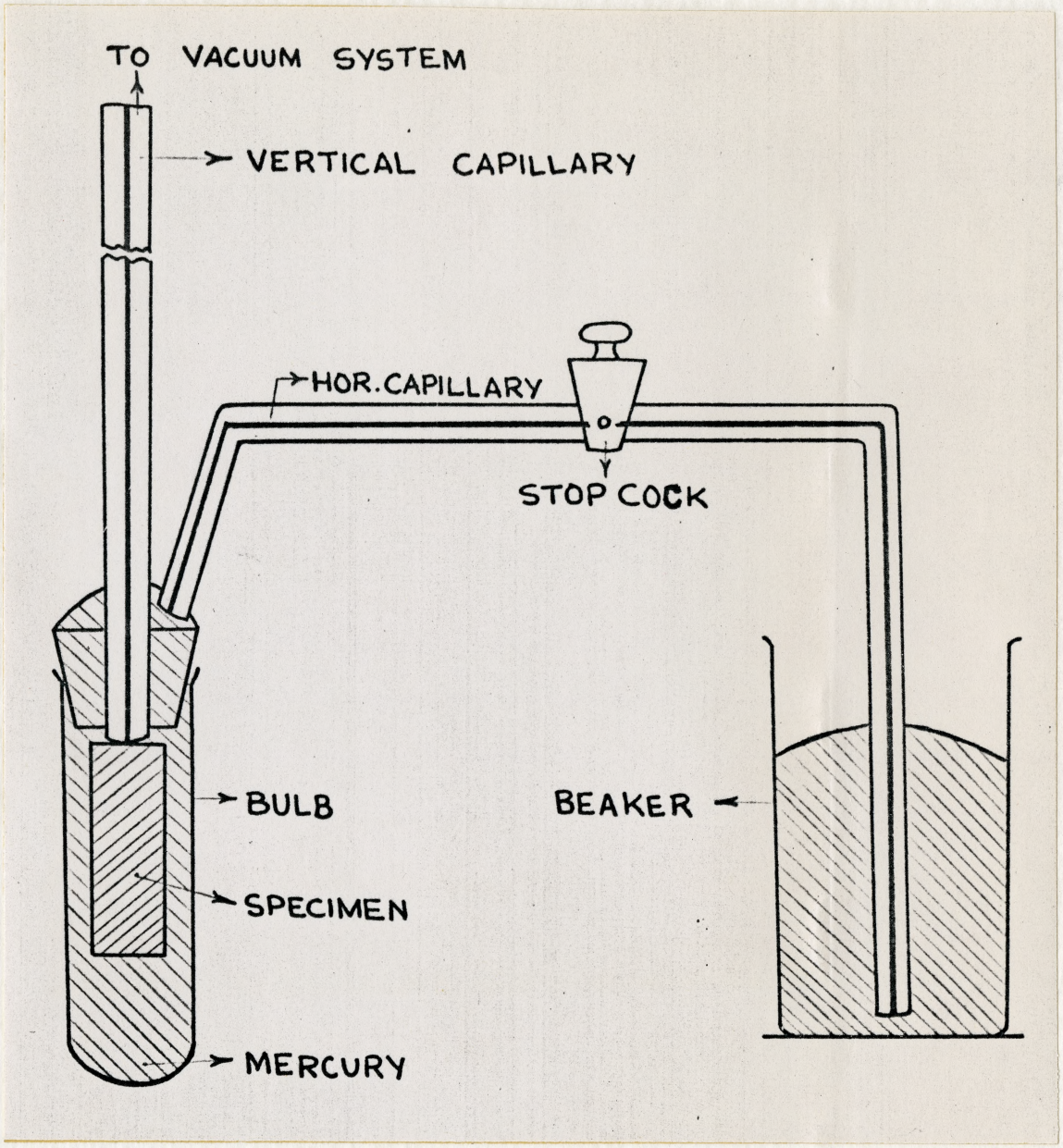

Figure 26

Mercury dilatometer for volumetric measurements.

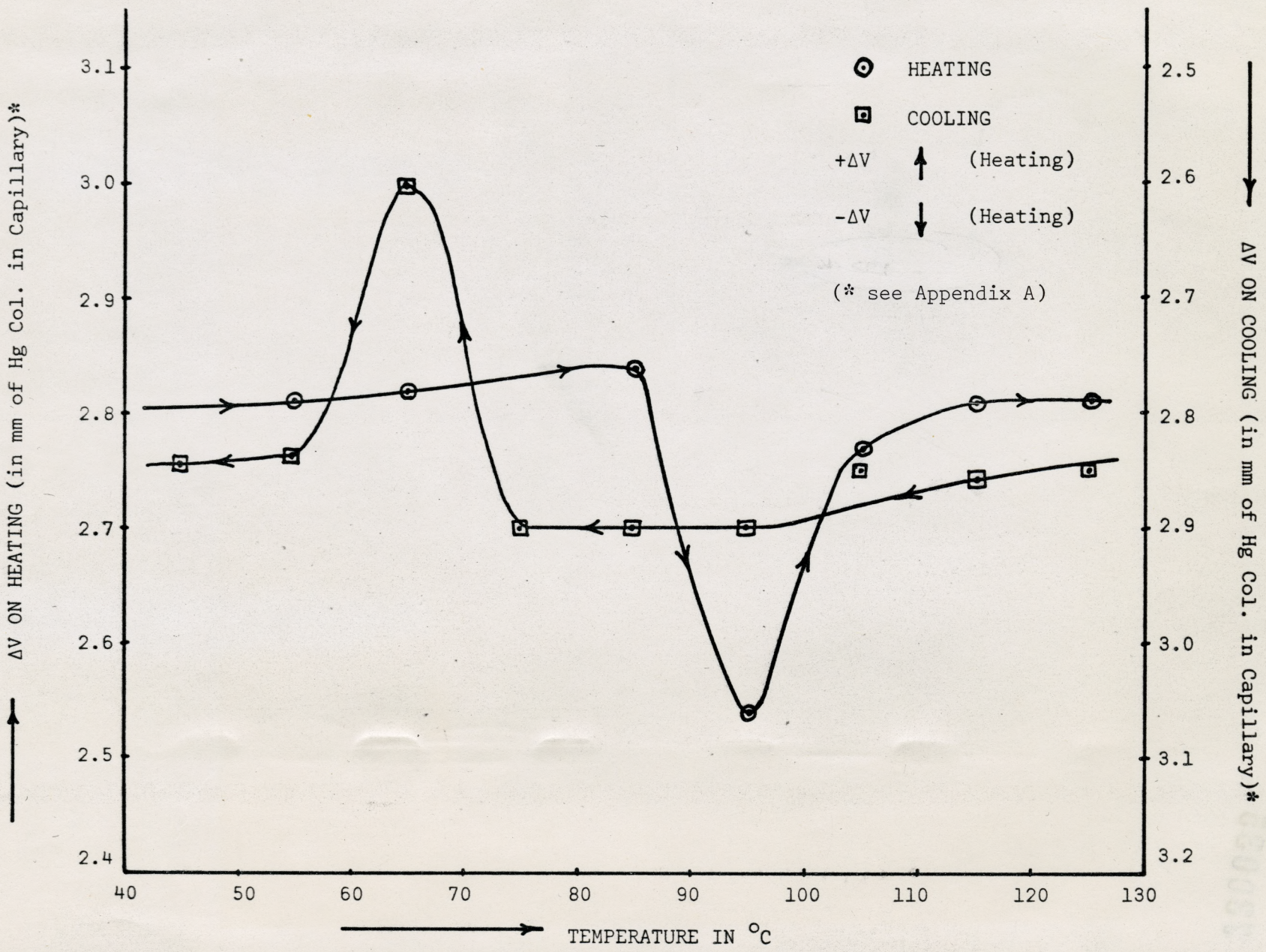

Fig. 27 Volume changes on heating and cooling a 50 at.% Ni alloy